NASw-4435

PowerSat

A Technology Demonstration of a Solar Power Satellite

University of Alaska
School of Engineering
Fairbanks, Alaska
1994

TECHNICAL EDITING & PUBLICATION DESIGN
Douglas L. Sigler
Zookerman Communications
P.O. Box 80649
Fairbanks, Alaska 99708
907 474-8053

COVER DESIGN
Cindy Nafpliotis

UNIVERSITY OF ALASKA FAIRBANKS

PowerSat

The Design Team

John Riedman – Project Manager
Jon Duracinski – Microwave Generation and Propagation
Joe Edwards – Attitude Control Engineer
Garry Brown – Communication Engineer
Ron Webb – Power Systems Engineer
Mike Platzke – Telemetry Systems Engineer
Xiaolin Yuan – Thermal Systems Engineer
Pete Rogers – Configuration Engineer
Afsar Khan – Spacecraft Structural Designer

Shawn Houston – Teaching Assistant
Dr. Joseph Hawkins – Faculty Advisor

Acknowledgments

The PowerSat design team would like to recognize the assistance received from a variety of sources. PowerSat was designed by the dedicated effort of ten students over the course of one semester, but received valuable insight from the efforts of the WISPER project, which was last year's USRA/ADP project at UAF. Their project was a springboard for research in the area of WPT and SPS.

We would like to thank William Brown, who pioneered WPT at Raytheon, for providing valuable mentoring to our microwave experiment during the semester. His knowledge of new advances in the field help to direct our efforts in the search for microwave sources and rectenna technology. We would also like to acknowledge his assistance in refining this proposal by being a member of the review committee during our critical design review.

We would also like to thank Rhonda Foster and colleagues at Tracor, Incorporated in Austin Texas. Their assistance was essential to the design of the deployable structures for this mission. They worked with our initial phased array design to best utilize all of the benefits of inflatable technology. They were always willing to discuss new options with our design team and to answer any questions regarding specifics of inflatable technology.

We would also like to thank Douglas Sigler, who volunteered his time and Zookerman Communication resources to turn individual technical reports into this completed document.

The PowerSat team would also like to thank the following members of industry and academic advisors who provided support and information about specific components for our project. We would like to thank:

Sheila Bailey	NASA Lewis, Solar Cell Technology
Doris Britton	NASA Lewis, NiH_2 Batteries
Dr. Charles Mayer	University of Alaska Fairbanks Microwave Technology
Ron Diamond Dimitri Krant	Spactralab, Photovoltaics
Bill Wise Jeff Dermott	Eagle Picher, Batteries
Bob Freeman George Sevaston	JPL, Attitude Control
Joseph Mack	Harris Corporation

Contents

SECTION 1 INTRODUCTION

PowerSat is a preliminary design strategy for microwave wireless power transfer of solar energy. Solar power satellites convert solar power into microwave energy and use wireless power transmission to transfer the power to the Earth's surface. The PowerSat project will show how new developments in inflatable technology can be used to deploy solar panels and phased array antennas.

This introduction will cover the justification for solar power satellites, hence our PowerSat project; review the criteria for our design; and introduce the manner for the design review.

HISTORY

The history of solar power satellites began as an application of wireless power transmission (WPT), studied in the early 1930's by Mr. H. V. Noble of Westinghouse Laboratory, and re-examined in 1959 by the Raytheon Corporation.[1] In 1968, Peter Glaser proposed using wireless power transmission to provide Earth's energy needs using geo-synchronous satellites. The satellites would collect solar energy using photovoltaic arrays and transmit it to the Earth in the form of microwave radiation. In 1977, NASA and the US Department of Energy (DOE) conducted a study of a 5 GW reference Solar Power Satellites (SPS) system.[2] Momentum for SPS lulled after the National Academy of Sciences recommended against implementation. The SPS '91 Conference in France demonstrated a renewed interest, as almost 100 papers were presented on the subject.[3] In 1992, the International Space University followed with a summer session in Kitakyushu Japan on the development of a Space Solar Power Program. The Japanese have shown a renewed interest in SPS, recently launching sounding rockets with their MINIX and ISY-METS experiments.[4] These launches are a part of a solar power feasibility study by a collection of their national agencies. In 1994 a delegation from the Japanese Ministry of International Trade and Industry (MITI) traveled to the University of Alaska Fairbanks (UAF) to present a comparison to the NASA reference study plan using new technology. The history listed above, influenced the choice of the solar power satellite, PowerSat, as the 1994 UAF ADP project.

PowerSat takes the next step in SPS development. The project represents the logical progression from the 1993 ADP at UAF: project WISPER, a study of Earth-to-Space WPT. PowerSat studies Space-to-Earth WPT. This project tests SPS concepts using current or near term technology. It demonstrates how advances affect some of the known difficulties such as large array deployment. The PowerSat project also provides the opportunity to conduct experiments concerning the effects on the atmosphere from a small scale SPS. PowerSat advances SPS science, a technology that holds promise of providing "clean" energy worldwide.

The Reference System

The reference system compiled by NASA in 1977 included the following components[5]:

a) Transmission of 6.78 GW
b) Use of 97,056 70 kW Kyltrons
c) 102 km^2 solar array (21280 m by 5385)
d) 7.3% efficient Si solar cells
e) Rectenna array on the ground measuring 204 km^2

This reference system is called the global scale model throughout the design. PowerSat's goal is to test current technologies that will influence the design of this reference system, and provide data to further its progress.

JUSTIFICATION

The idea of solar power satellites is not new, however, to put the project into perspective it may be necessary to compare some hard numbers. When ten billion people inhabit the earth, and if everyone consumes as much energy as the average American, 10 kW, the power requirements for the world will be 100 terawatts. The comparison between straight solar power and a global model of a solar power satellite is shown in table 1-1 under clear sky conditions.

Table 1-1 Solar Power to Global Model Comparison

	Solar Panels	Solar Power Satellite
Power incident from Sun (kW/m^2)	1.0	1.4
Efficiency of Solar Cells	15%	15%
Effective Area	25% .5 day and night .5 incident angle	100%
Maximum Power Density (W/m^2)	37.5	Assume 1000
Area Receiver on Ground (m^2)	2.7 x 10^{12}	10^{11}
Circular Diameter of Receiver (miles)	1152	220

The global model produces all of the world's energy requirements, alleviating constant depletion of natural resources. The environment is preserved because the energy necessary to recycle is available. However, size of the global model satellite requires international cooperation.

Comparison of Solar Array with Rectenna Array

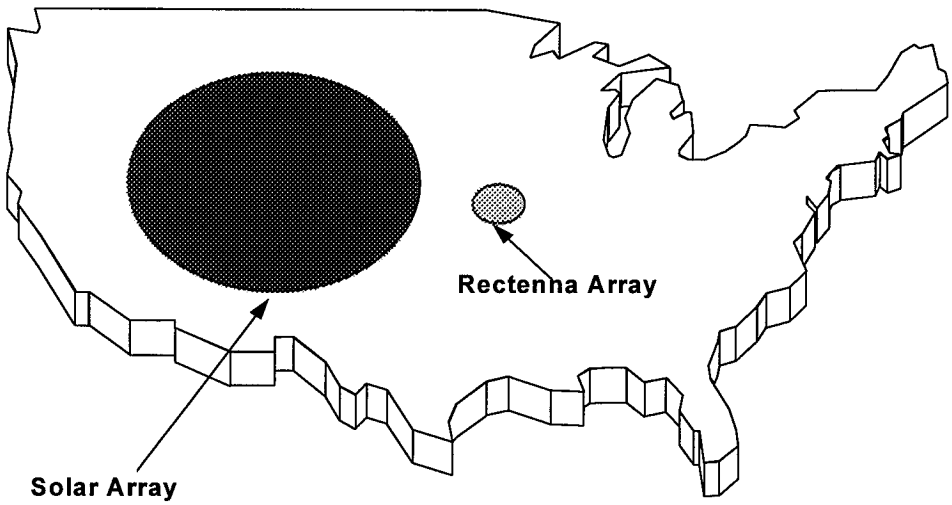

PowerSat is a scale model of the global model, testing proof of concept and giving global model experimental results. In order to provide necessary global scale results, the PowerSat project is designed to provide a variety of experimental data. PowerSat allows the possibility of beaming to multiple ground sites by using electronic steering on the phased array, and by utilizing mobile ground stations for the collection of data in different environments. This capability enables PowerSat to provide valuable information for the global model design.

DESIGN CRITERIA

Global scale model criteria was used to design the small scale PowerSat prototype. PowerSat's design criteria include: using current technology either available or attainable in the near future, proving the concept of solar power satellites and attaining meaningful experimental data, keeping the overall cost of the project on the national scale (under $500 million), testing emerging technological advances in the field of solar power satellites, and maintaining global model scalability. PowerSat's design team used these criteria as project guidelines and constraints.

INTRODUCTION TO THE DESIGN

PowerSat demonstrates the use of inflatable technology both as a means to deploy and rigidize large solar arrays, and a method for designing a large transmitting phased array antenna. PowerSat beams 100 kW, considerably less than the global scale will generate; and will collect data in a variety of environments using a mobile ground station. The experiments include testing the effects of high power propagation through the ionosphere for both daytime and nighttime conditions.

Expansion of the design to a global project involves increasing the order of magnitude of the total power collected, providing a proportional increase in beamed power. PowerSat costs less than $100 million, and provides a representative wireless power transfer experiment with global model scalability.

SECTION 2 MICROWAVE POWER

MICROWAVE POWER EXPERIMENTS

MICROWAVE EXPERIMENT OVERVIEW

Microwave Overview

Information, skills, and equipment from many fields are necessary to provide wireless power transfer from the planet's orbit to collection stations on the planet's surface. This project makes use of existing technology and knowledge to further explore the possibilities and effects of wireless power transmission to Earth. Much of the microwave equipment in the project has not yet been proven in a space environment. Wireless power transmitting experiments are planned during the project's operational phase.

The first step in this process involves incident solar energy conversion to a direct current (DC) voltage suitable for input to a microwave source. This source then converts the energy to radio frequency (RF) energy. The energy is transported via waveguide to an antenna which transmits the energy as a directed beam towards planet surface collection sites. Several effects cause a decrease in the amount of energy in the beam as it propagates to the surface. Study and prediction of these propagation losses are reviewed in detail later in this section. At the collection site, the beam is converted from RF to DC, which can be used or stored.

Experimental Objectives

Microwave Source

RF to DC testing and operation is a major objective for the PowerSat project. This experiment consists of controlled variations of the time duration the source is generating RF energy, and of the input voltage and current to the microwave source. Accurate results for this experiment are based on variables, such as atmospheric conditions and the distance between the antennas. To determine operational characteristics in the space environment, this data is compared to ground control experiments. Results from these experiments will improve future microwave source reliability and efficiency.

Phased Array Antenna

This project proposes using a phased array as a transmit antenna. Several concepts utilized in the antenna design have not been previously applied in this manner.

Analysis of the transmit array operating properties enable improvements on future designs. A complete discussion of the phased array and its properties to be studied are covered in a later section.

Propagation Effects

Large scale power transmission from orbit could cause changes in the medium through which the beam passes. For this reason, several experiments concerning ionospheric and atmospheric effects is completed. Propagation effects statistics is collected during the course of the experiment to provide as broad a statistical picture as possible. The objective for these experiments is to determine what are the effects of power transmission from orbit. Figure 2-1 shows various layers in the atmosphere.

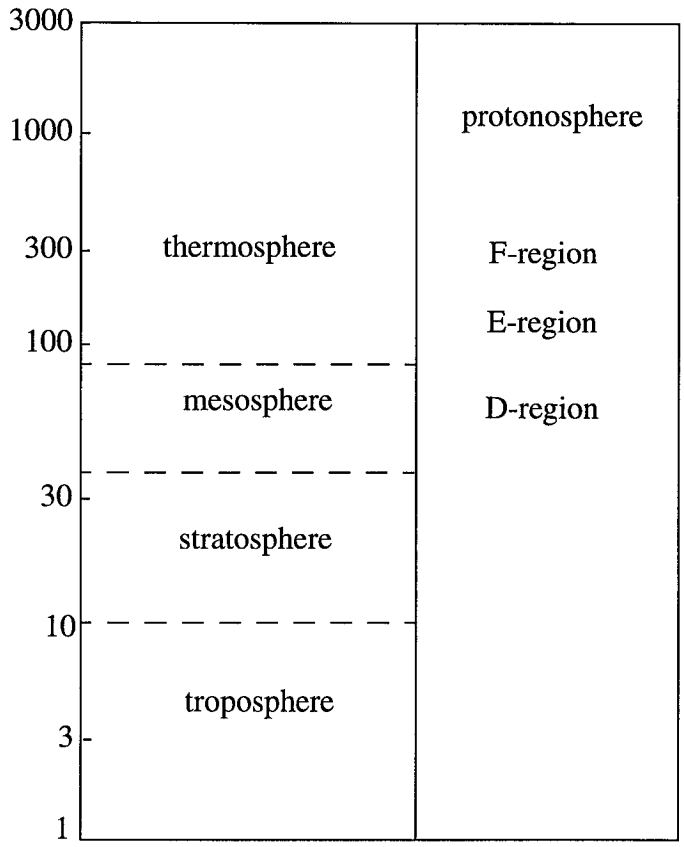

Figure 2-1 Primary categories of the Earth's atmosphere (Allnut)

Ionospheric Effects

To study the power beam effects on the ionosphere's total electron content (TEC), the beam's Faraday rotation is measured under as many different conditions as possible. Particular areas of interest are diurnal (day to night) variations, seasonal changes, and various sunspot activity intensities.

The information gathered on TEC is used to adjust the ground station's antenna polarity for maximum power reception when data on Faraday rotation is not being recorded.

Atmospheric Effects

Troposcatter communication link experiments are planned. Links is established through various atmospheric layers to determine if the beam passage causes atmo-

spheric heating, or changes that will interfere with other RF spectrum users.

Troposcatter equipment can be purchased from the military, but it is possible that the equipment can be leased. Other types of communications equipment experiments are being considered to provide data for a broader frequency range.

Ground Station
Ground collection station property studies will determine possible future implementation upgrades. The collection station and its properties to be studied follows the phased array discussion. At the ground station, experiments can be conducted for multipole tests and low power rectennae.

FREQUENCY SELECTION

The project's wireless power transmission (WPT) operating frequency specification was chosen after considering trade-offs from the various available choices. A frequency was chosen by analyzing current microwave source technology, operating frequency effects on the transmit and receive antenna characteristics, and propagation losses for a transmitted beam at the available operating frequencies. These factors are interrelated as shown in figure 2-2.

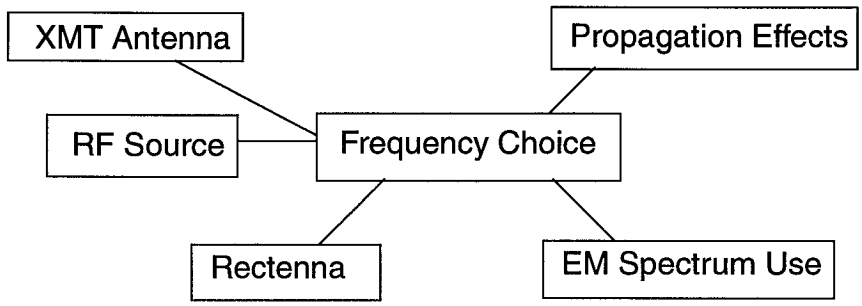

Figure 2-2 Block Diagram of Design Options

Microwave Source Options

We examined current technology RF sources and found a source based on the following parameters:

Output Power
A specific microwave power density is required by the rectenna for operation and efficient energy conversion. To meet this goal, but remain within PowerSat's small scale demonstration goal, a microwave source that can output a few tens of kilowatts is required.

DC to RF efficiency

A high DC to RF conversion efficiency is important to keep the required DC power to a minimum. Current sources available are represented on the high end by magnetrons, with a conversion efficiency of 70-90%. Tube sources, such as Klystrons and Gyrotrons, typically have efficiencies of 30-40%. Solid state sources currently operate at the 25-40% efficiency.

Waste Heat Generation and Elimination

Waste heat generation is directly related to the DC to RF conversion efficiency. The more efficient the conversion process, the less waste heat produced.

Another important factor is the operating temperature. In space, waste heat can only be lost through radiation. Radiative heat loss is a temperature function to the fourth power[1]. Thus, a high operating temperature is desirable. In general, tube amplifiers operate at a much higher temperature than solid state devices.

Mass

Low mass is important when objects are being placed in earth orbit. Under this criteria magnetron[2] and solid state sources have the advantage. Usually, sources such as gyrotrons, with the desired power outputs, require heavy magnets and/or active cooling systems for operation.

Interference

The operating frequency band must be chosen so that operation will not cause unacceptable interference with other RF spectrum users. The 2.45 and 5.8 GHz frequencies are desirable because of Industrial, Scientific, and Medical (ISM) bands located around these frequencies.[3]

Microwave Source Determination

Based on the above criteria, and the ability to demonstrate a technology that can be upscaled for a global system, we chose the magnetron at the 2.45 GHz operation frequency. Final DC to RF converter selection did not take place until antenna and propagation considerations were analyzed.

Frequency Dependent Variables

Trade-offs are inherent to the frequency choice. Using microwave source data, the following items were assessed to determine the operation frequency:

Beam Width

The beam spot size on the planet becomes smaller as a function of frequency. The higher the frequency, the narrower the beam width, and the more power that is delivered to a specific area. A feasible rectenna size, considering this project's intended scope, was considered in selecting a frequency. The beam width is also dependent on the transmitting antenna's size.

Size of Transmit Antenna

The required transmitting antenna's size is related to the operating frequency.

$$A = \frac{\lambda^2 \cdot G}{\eta \cdot 4 \cdot \pi} \qquad \text{(eqn. 2-1)}$$

where

A is the Area
λ is the wavelength
G is gain
η is efficiency

Operating frequency parameters that produce acceptable values for available gain, while maintaining a feasible structure size, were evaluated. A minimum gain for this demonstration was established. A global system antenna could be made as large as needed to obtain necessary gain, and the size of the solar array would more than likely be much larger.

Orbital Height

A system's free space loss increases as a distance function. Above certain altitudes, the system size required to deliver adequate power to the rectenna would be beyond this experiment's scope. Below a certain orbital altitude, the mission life would not be long enough to obtain adequate experimental data.

Propagation Effects on Beam

Propagation effects evaluated at various operational frequencies are covered in this section. Models to evaluate propagation effects cover the Faraday rotation, free space loss, and gaseous attenuation effects on the microwave beam at representative frequencies under clear sky conditions with a 50% relative humidity. The assumed elevation is 600' above mean sea level (AMSL) and the ambient temperature is 15°C.

Ionospheric Effects

Plasma/Critical Frequency

Radio wave absorption and refraction in the ionosphere decreases as the frequency increases. The effects become negligible above 1 GHz. For this reason, there is no allowance for loss due to the plasma/critical frequency.

Faraday Rotation

Faraday Rotation is the rotation of a linearly polarized vector about its propagation direction when passing through the ionosphere. The effect is represented at zenith by the following equation:

$$\phi_i = \frac{2.36 \cdot 10^4}{(f)^2} \times Bav \times TEC_i \times rad \qquad \text{(eqn. 2-2)}$$

where

f is frequency
Bav is Earth's magnetic field
TEC is electron content

Figure 2-3 shows the diurnal and slant path induced polarity rotation.

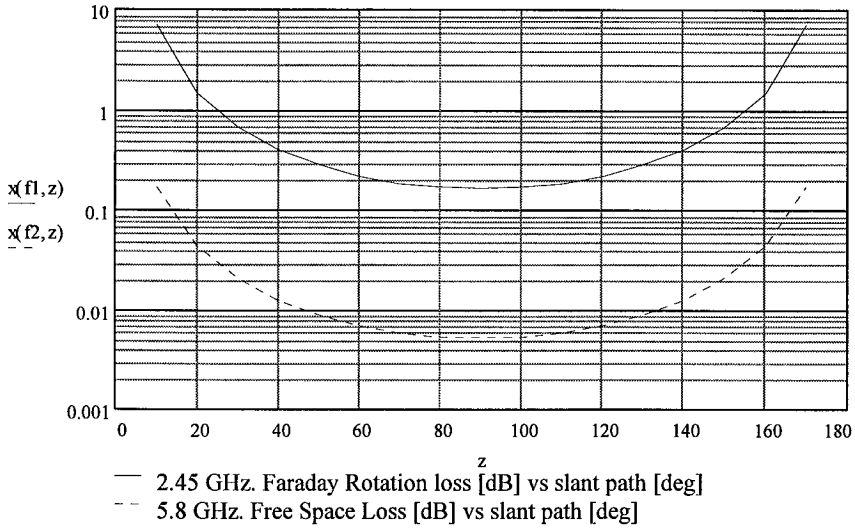

Figure 2-3

The loss caused by Faraday Rotation is shown on the ordinate, and the slant path angle is on the abscissa. The range of loss induced by Faraday Rotation at 2.45 GHz varies from 0.166 dB at zenith to 7.23 dB at 10° from the horizon. The effect on the beam at 5.8 GHz falls in a range of 0.005 dB at zenith to 0.175 dB at 10° from the horizon. Faraday Rotation effects at higher frequencies become neglible.

To minimize the loss due to Faraday Rotation, an optimum offset angle for the receive antenna is determined experimentally under various conditions. The mitigation of loss due to Faraday Rotation is analyzed for effectiveness. Anticipating less than 1 dB loss from Faraday Rotation after offset implementation, this effect will not be included in the total expected path loss.

Free Space Loss

Loss Due to Free Space Transmission

The free space loss is calculated as follows:

$$PL(z) = \left[\frac{4 \cdot \pi \cdot h(z)^2}{\lambda}\right] \qquad \text{(eqn. 2-3)}$$

where

h is separation

A graphical representation of the expected free space loss is shown in figure 2-4.

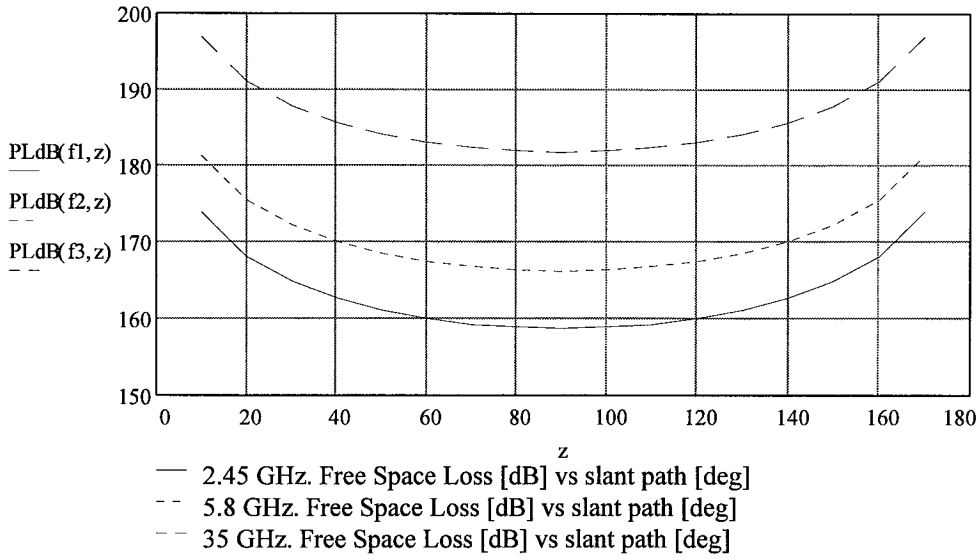

Figure 2-4

In the preceding graph the free space path loss in dB is on the ordinate, and the slant path angle in degrees is on the abscissa. The zenith free space path loss at 2.45 GHz is 158.7 dB, and the slant path free space loss at 10° from the horizon is 173.902 dB. The free space loss for a 35 GHz and a 5.8 GHz beam are represented by the top and middle curves, respectively.

Tropospheric effects:

Clear Sky (Gaseous Attenuation) effects:

Equation 2-4 is used to calculate the gaseous attenuation.

$$A_g(f, z) = \frac{\gamma_o(f) \times h_o e^{\frac{hs}{ho}} + \gamma_w(f) \times h_w(f)}{\sin(\theta(z))} \qquad \text{(eqn. 2-4)}$$

Figure 2-5 shows the expected gaseous attenuation at 50% relative humidity at 600' above sea level.

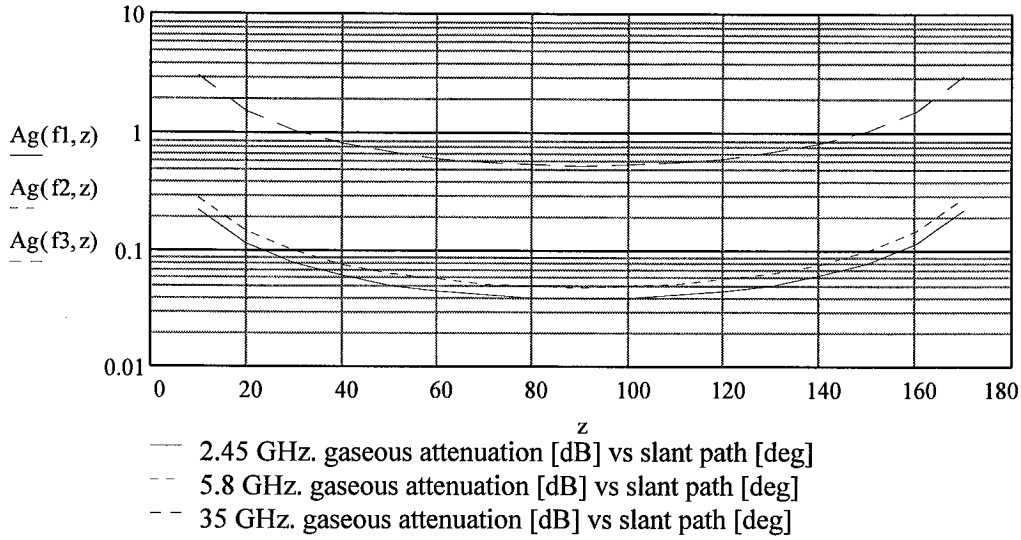

Figure 2-5

The bottom curve shows the loss for a beam at 2.45 GHz. The gaseous attenuation for a 35 GHz and a 5.8 GHz beam are represented by the top and middle curves, respectively. There is a large increase in loss when moving from a 5.8 GHz beam to a 35 GHz beam.

Total Expected Beam Loss

The total expected beam loss under clear sky conditions is determined by totaling the losses, due to free space loss and gaseous attenuation along the slant path. As previously stated, the loss due to Faraday Rotation is negligible. The total loss is shown in figure 2-6.

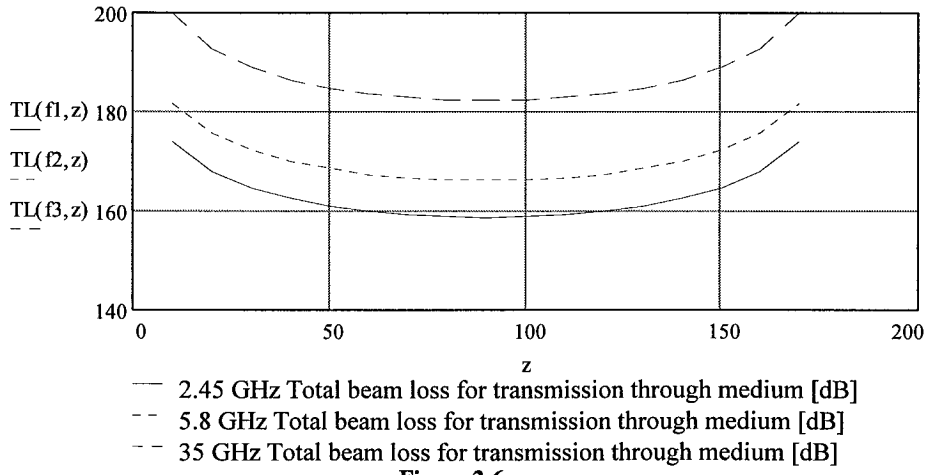

Figure 2-6

The graph (figure 2-6) shows that the increase in propagation loss for the 5.8 GHz and the 35 GHz frequencies, over that of the 2.45 GHz frequency, is approximately 7.5 dB and 24 dB, respectively.

Conclusions Concerning Propagation Losses

The frequency of operation that most effectively delivers power is 2.45 GHz. At frequencies above 10 GHz gaseous attenuation becomes a large loss factor. A 35 GHz beam would be attenuated by cloud cover or precipitation, limiting the usefulness of the system under conditions that were not optimal.[4] Predicted loss under moderate rainfall conditions ranges from 5 to 10 dB.

A beam at 2.45 GHz would experience the least propagation losses. For this reason, propagation considerations show an advantage to using the lower frequencies when beaming power through the Earth's atmosphere.

Frequency of Operation

Analysis of the above variables led to a 2.45 GHz frequency of operation choice. A modified magnetron is the microwave source. This magnetron is shown in figure 2-7. Antenna design and specification in the following sections was completed using this frequency.

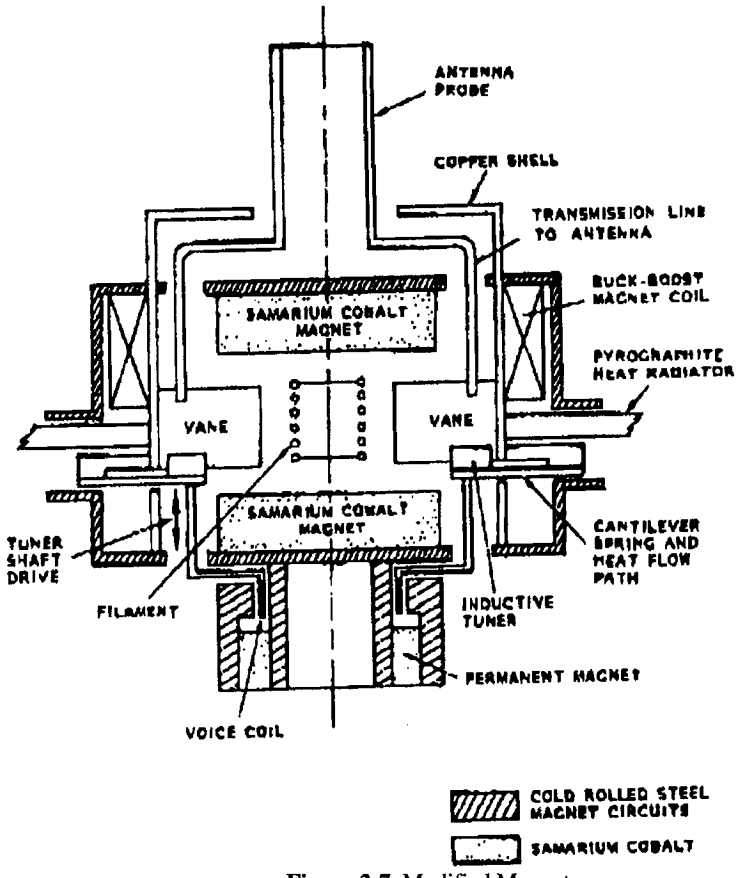

Figure 2-7 Modified Magnetron

Parameters

The following list contains the design choice parameters for a microwave source to implement the DC to RF conversion. The information below is for a single modified magnetron. The satellite transmission system is configured for thirty-two magnetrons feeding a single phased array antenna.

Operating frequency
f = 2.45 GHz

Power output
P_t = 3.2 kWatts

Conversion Efficiency
η = 85%

Waste heat dissipation
T = 300 C° operating temperature
Passive radiation to space

Magnetic field
1500 gauss

Mass
m = 1.018 kg (Estimated)

RF Source, Frequency Choice Summary

The amount of RF power produced, and the propagation losses predicted, are shown in Table 2-1. The loss values reflect predictions for zenith.

Table 2-1 RF Power Produced and Propagation Losses

Power Per Magnetron	3200 Watts
Number of Magnetrons	32
Transmitted Power	102.4 kilowatts
Transmitted Power (z)	50.10 dBw
Loss Atmospheric	0.03 dB
Loss Free Space	158.65 dB

The microwave source was chosen by considering the operating characteristics of available technology. Criteria assessed included RF to DC conversion efficiency, operating temperature, mass, power output, and reliability following the methodology of Brown.[5] The frequency choice was based on the RF source choices, spectrum use, and the effects of frequency on propagation effects and antenna properties.

A modified magnetron operating at 2.45 GHz, is the best source for the PowerSat project. The controlled phase and amplitude of the magnetron enable its use in a global scale system. The high power output to mass ratio of the magnetron makes the use of the magnetron in a global scale system attractive. Completion of this project will provide technical data for large scale use..

SPACECRAFT REQUIREMENT

Mission Requirements

The scalability of PowerSat guided the spacecraft design process. This scalability affects the following mission requirements:

a) Reduce orbital altitude from geosynchronous to low Earth orbit (LEO) to limit cost and payload size. Accept the shorter pass times as a limitation of the scaling.
b) Reduce total power beamed (from 6 GW for the global model to 102 kW for the prototype). Less power reduces the size of the solar array and the mass of the transmitter module.
c) Reduce the size of the transmitting array. A global power satellite would require a rigid transmitting array on the order of one square kilometer in area.
d) Utilize concentrators at the ground station to compensate for the reductions in received power level.

Phased Array Antenna

The design requirements for the phased array antenna developed from three factors:

a) A total power of 100 kw to be beamed from the satellite.

b) The minimum power density required to activate the rectenna diodes, the turn on power, which was estimated initially at 100 m W/m^2.

c) The total mass and volume of the phased array to meet criteria ***a*** and ***b*** above.

Using the total beamed power and the required power density at the ground site, it was determined that a concentrator is required at the ground station. Equation 2-5 estimate a value for the antenna gain.

$$Gain = P_R + FM + L_{FS} - P_T - G_R \qquad \text{(eqn. 2-5)}$$

The calculated values for the transmit power, receiver gain, and required receive power are calculated and used in this equation to give an equation for gain which relies only on the altitude of the satellite.

$$Gain = 1.00 + 3.00 + 158.95 - 50.10 - 46.00 \qquad \text{(eqn. 2-6)}$$

The equation for gain is then modified so the area of the array can be calculated for a given required gain.

$$A(R) = (\lambda)^2 \cdot \frac{G(R)}{\eta \cdot 4 \cdot \pi} \qquad \text{(eqn. 2-7)}$$

Where

A is the Area
G is the Gain as Function of Range
λ is the Wavelength [m]
η is the efficiency of the transmitting array

Figure 2-9 graphs the required gain for the transmitting array against the possible altitudes for the satellite, and the antenna size increase as a function of the orbital altitude. Obviously a rigid antenna required for even 800 km is too large for the scope of this experiment, however, much inflatable structures for space missions research and design is currently being done. For the 500 m^2 or larger array required for this experiment, an inflatable structure is ideal.

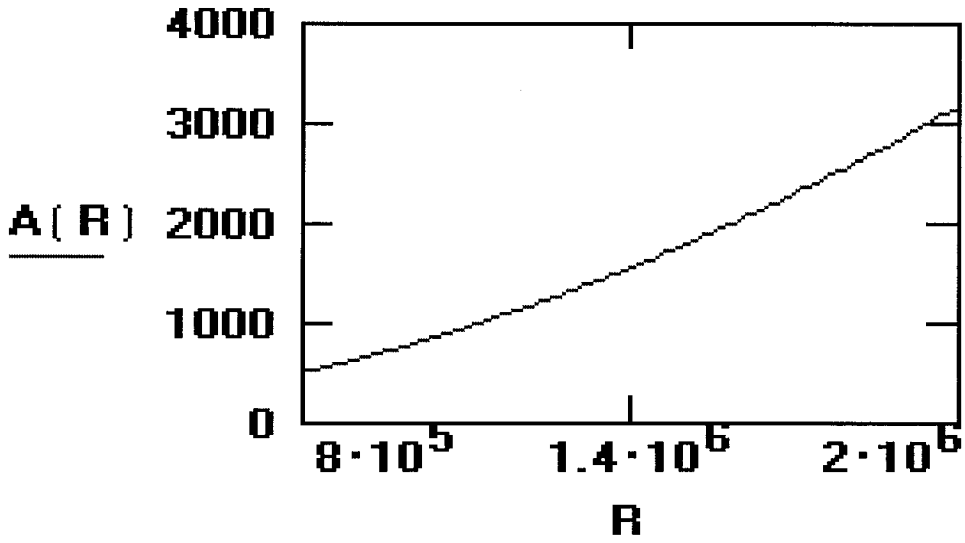

Figure 2-9 Antenna Size (Area) Required for Given Orbital Altitude

The PowerSat orbital altitude is at 835 km. This is the zenith distance to the satellite and is used to determine the area required for the array. Equation 2-7 yields a 554 m^2 array area. Allowing for atmospheric effects in the loss equation increases the area to about 575 m^2.

The array is rectangular to maximize the array's steerability, as discussed in the next section. The actual size of the array is set at 32 meters long by 18 meters wide, yielding a 576 m^2 total area.

As mentioned previously this area is too large to consider a rigid structure. Tracor, Incorporated, experts in inflatable structures, was consulted. They assessed this design to be within the scope of current inflatable structure technology. Specifications for the inflatable structure are discussed in section four.

Power Patterns and Pointing Accuracy

A rectangular phased array yields some specific advantages in aiming the microwave beam at a ground station. Using thirty-two separate magnetrons for the high power amplification, the phase shifts from them individually, and phase steers the antenna onto the target receiver. This electronic steering obviated a complicated physically steering system. Physical steering is difficult for a large inflatable structure since they are not rigid enough for rapid orientation changes.

The magnetrons are linked in pairs for the sake of system redundancy, allowing 100% backup on the high power amplification. This redundancy would be at a reduced power level, but will maintain the array's steerability in the event of a failure in a magnetron, or in the power systems. These 16 separately phased controlled array sub-elements are arranged as shown in figure 2-10. Each subarray is fed by a pair of magnetrons, and each pair is fed the 2.45 GHz phase shifting signal that adjusts the phase of the output to steer the transmit beam onto the target site. The long axis, which has the greatest freedom of steering, is aligned in the direction of the satellite's travel, maintaining the beam on the target during the overhead pass.

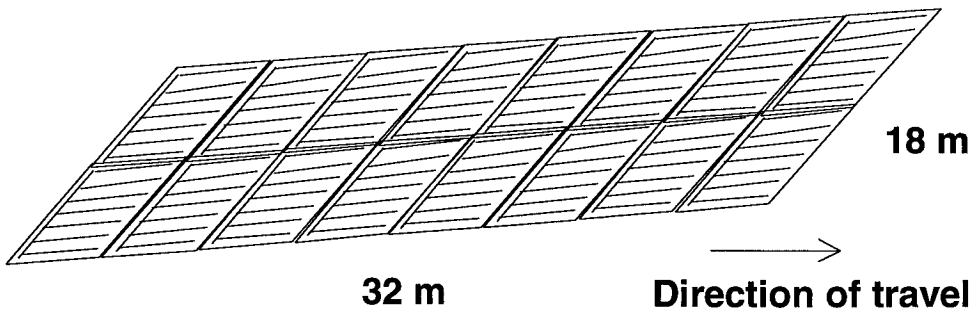

Figure 2-10 Phased Array Antenna

By using a linear polarization, array pointing is simplified further. Linear polarization yields maximum steerability for a slotted array and allows further increase in the gain of the antenna by adding Yagi-Uda passive directors to each of the array's slot elements. Four strips of titanium laminant are added perpendicular to the slot, spaced approximately ¼ wavelength apart.

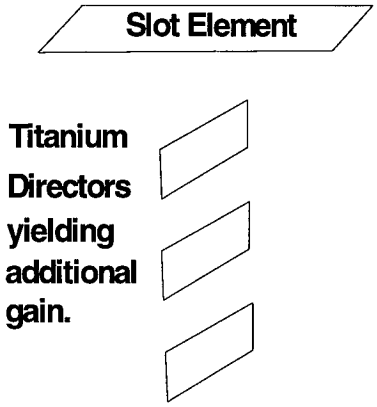

Figure 2-11 Passive Directors and Orientation with Slot Element

Based on this design, the array has the ability to steer up to 25° forward or behind its direction of travel, and up to 5° in either lateral cross-track direction. As long as the antenna remains oriented towards the Earth, the beam can be steered onto any target visible below it. This also gives PowerSat the ability to switch between target sites rapidly. Part of the experiment's objective is to evaluate this capability. Target sites is set up along the satellite path to evaluate PowerSat's ability to provide power to successive sites.

Design limitation is due to quantization levels in the phase steering of the beam. The phase shifting used to steer the beam is limited to the 16 subarrays which constitute the full array. Since each of these subarrays have the same phase, varying the phase to steer the power beam results in a step function rather than maintaining linearity. These steps become great enough that spurious sidelobes (quantization levels) are produced. The result is that less power is supplied to the main lobe and the main lobe itself is distorted. This distortion limits the array steering angles.

$$\frac{d}{\lambda} < \frac{1}{1 + \sin\theta_s} \qquad \text{(eqn. 2-8)}$$

These steering limits greatly impact the attitude control of the array as discussed in section four.

GROUND STATION REQUIREMENT

Ground Station Overview

Ideally, the wireless power demonstration would result in a ground based antenna collecting all of the power transmitted at 2.45 GHz from the sun synchronous satellite. However, most of the power is lost in free space dissipation over 835 km. Other power is lost in gaseous attenuation in the atmosphere. The power that does reach Earth is very diffused, and only a fraction can be contained in any reasonable receiver area.

From the ground station perspective, a receiver must be large and efficient enough to capture a notable amount of energy, yet meet geographical and political constraints. Its objective is to collect some of the power density incident at 2.45 GHz, and produce a representative DC voltage. Figure 2-12 shows a block diagram of the general aspects of the power receiver.

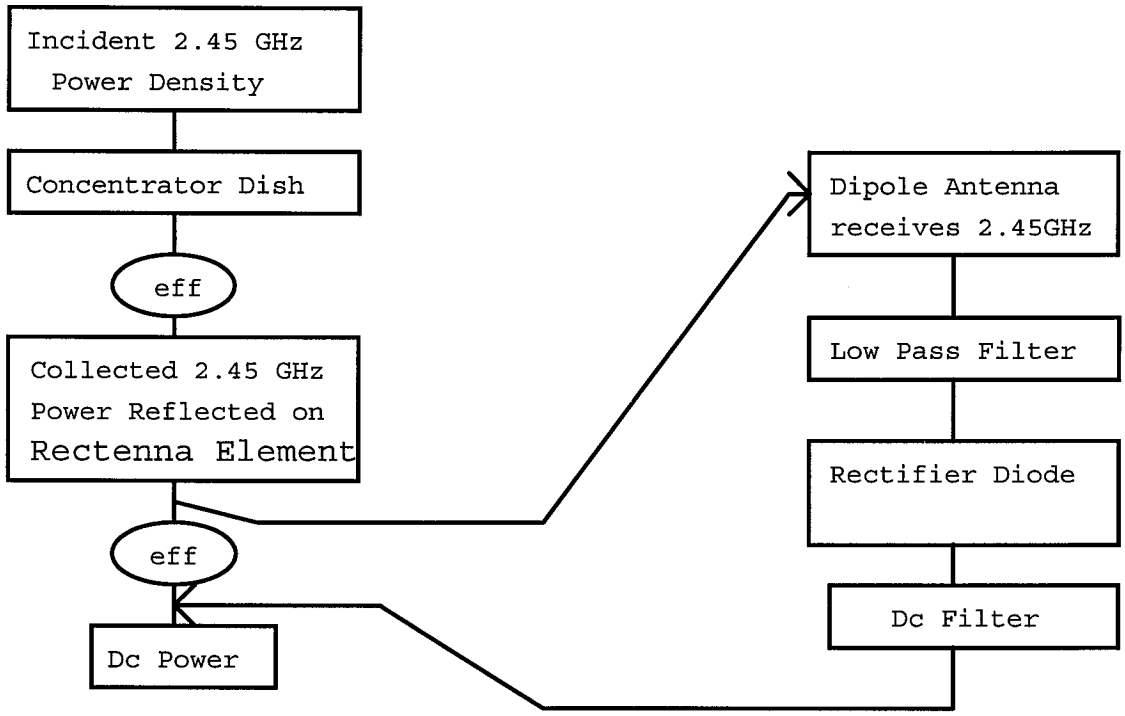

Figure 2-12 Block Diagram of the Receiver

Ground Station Requirements

The Earth Station is expecting a power density of about 56mW/m^2 at a 2.45 GHz frequency. The incoming wave will have linear polarization. It is expected to pass over the station once every 1.5 days for 7.8 minutes, and make subsequent 4 minute passes every other 12 hours. Power is beamed for 6.2 minutes each day on the longest pass. Tracking is necessary, and with the current power densities, a concentrator is necessary. It is feasible to exclusively use a low-power density multidipole rectenna array, but the incident power just meets the multidipole array requirements, resulting in low efficiencies.

Ground Station Location

The ground station is located at White Sands Testing Facility. The climate and weather are mild, precipitation is relatively low, and ground obstructions are minimal. This facility also is the downlink from the TDRSS communication satellite, so information is readily available to our station. Other likely considerations were the Kimberly Plateau, Australia and the Nubian Desert, Africa. The White Sands is an

ideal location for the initial site because of its telemetry convenience, relatively good atmospheric conditions, and political simplicity.

The Rectenna Array

Rectenna Element

A rectenna is an antenna and a rectifier acting as a RF to DC power converter. A half-wave dipole is typically used as the antenna, thereby limiting the system to linear polarization, usually on the order of 100-140 ohms. The dipole antenna is not designed for full-space orientation, so a grounding plane is used, extending well beyond the end element (at least 1λ) to avoid effects on the radiation pattern.

Rectenna Construction

The Schottky Barrier Diode (SBD) serves to rectify the incoming waveforms into a DC signal. The diode is most often made from Gallium Arsenide (GaAs) for its low resistivity and its low conductivity when undoped. The substrate is semi-insulating, resulting in simplified insulation of other associated devices and a smaller capacitance between the devices and ground. The n-type SBD does not exhibit minority-carrier storage effects and reveals only capacitative effects from the depletion layer. It has a very low series resistance and junction capacitance without giving up reverse breakdown voltage or power handling. The SBD is constructed like a MESFET and has an identical i-v relationship as a pn junction with characteristic values of $Rs < 4\ \Omega$, $Cjo = 0.07$ pF, and $Vbr \approx 6$ V.

Rectenna Circuit

The rectenna diode prefers a 3-10 Ω input impedance, and a 250 Ω load. In addition, it works under the assumption that the high order harmonics are not present to interject noise and heat, so filters are heavily weighted. A low pass filter is necessary between the antenna and the diode to match impedances and pass only the fundamental frequency and less (DC). A DC-pass filter is used between the diode and the load to confine higher harmonics and pass only constant non-oscillatory power. Figure 2-13 shows a typical rectenna circuit.

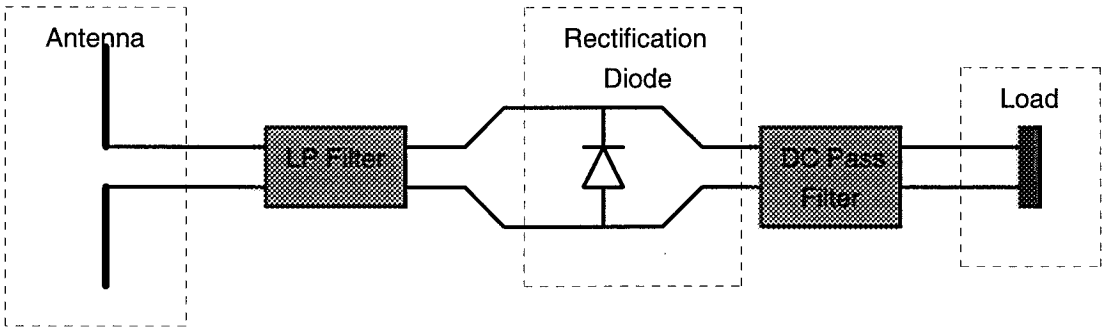

Figure 2-13 The Rectifier Circuit

The most frequent sources for power loss are due to antenna mismatching and diode dissipation. The antenna matching is particularly critical with a multi-dipole design because there are many individual dipole elements with distinct impedances for each

diode. The diode losses are typically caused by poor filtration, resulting in a harmonic caused voltage drop across the diode. Also the series resistance of the diode or junction capacitance may not be negligible. At higher frequencies, such as 98GHz, rectenna elements display additional power losses within the circuit connections themselves, bringing overall efficiencies down.

The Rectenna Array

A typical rectenna element prefers an operating range of 1-10 watts, and with a concentrator, it is feasible to effectively power one rectenna element. However, it will not demonstrate the most efficient method for much of the density is wasted when only powering one dipole. A new type of rectenna element is shown in figure 2-14, however it is constrained to a linear phase front. This is due to the joint rectification circuit for the multiple dipoles. Hence, any nonlinearities in phase on the entire dipole set will cause the incident signal to add constructively and destructively, with the fringes of the array yielding very poor power output and the overall efficiency being extremely low.

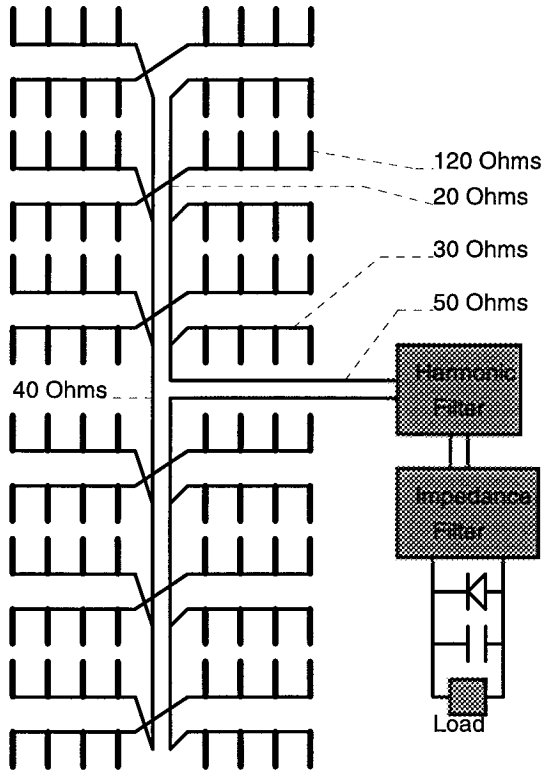

Figure 2-14 The 48 Dipole Array

The latest development involves multiple dipole antennas for each diode circuitry. However, due to the array's necessity for a linear phase front, efficiencies of only about 50% have been achieved practically with a incident linear polarized wave. With expected linear polarization, this array would be good, but, any reasonable

attempt to collect the incident power and reflect it upon the array will lead to destructive patterns upon the array itself, due to the non-linearity of the reflected beam. The multidipole array operates in densities 10^4 times less than conventional elements, which is certainly incentive to look for future methods to improve efficiency and perhaps make it immune to independent dipole phase differences. William Brown from Raytheon Company, addresses this rectenna array in "A Transportronic Solution to the Problem of Interorbital Transportation" (p.107).

A future consideration may be to place the 48 dipole rectenna directly upon the incident power when suitable densities can be provided. Alternatively, a linear phase reflector could be devised and aligned with the satellite's polarization and orbital path, like a cylindrical parabolic reflector.

Due to the present conditions, the ground station is constrained to a single dipole rectenna element placed within the focal beam of a 9 m diameter parabolic reflector dish. Figure 2-15 is an illustration of the power collection process. With the expected incident power density of 56 mW/M^2, a parabolic efficiency of 75%, and a rectenna element efficiency of 80%, the output DC power should be approximately 2.15 watts.

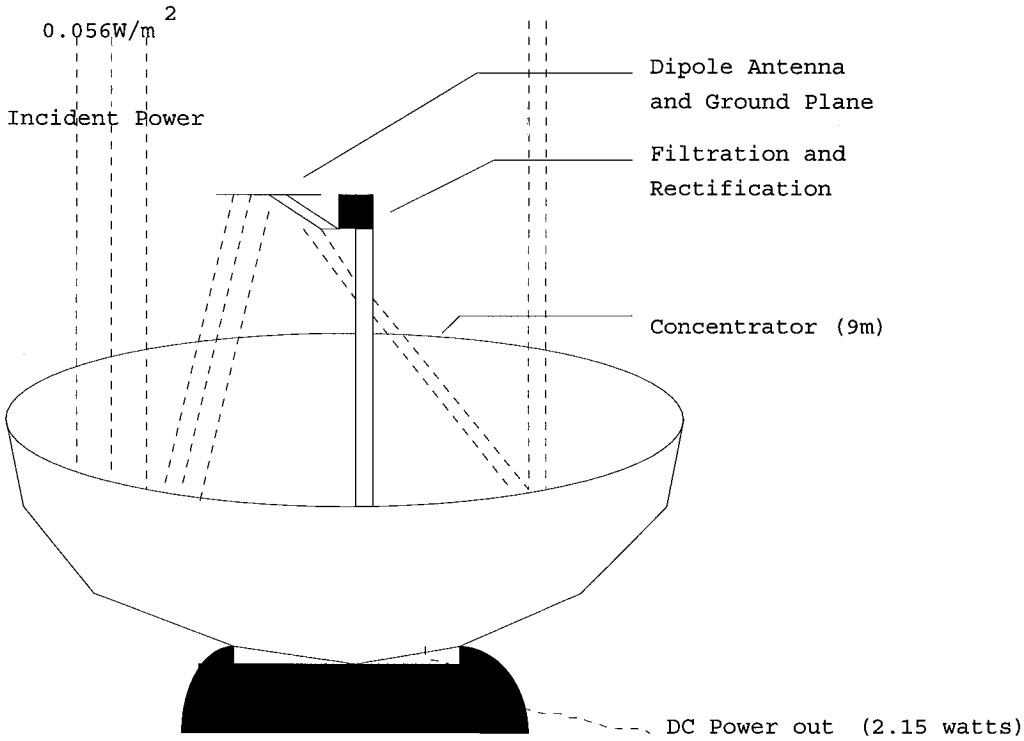

Figure 2-15 Power Collection

Concentration and Tracking

Concentrator

The rectenna element is placed completely within the focal beam of a parabolic dish, 9 meters in diameter. The dish will concentrate the incident power onto the rectenna plane with efficiencies of 75%. This collector can be purchased from Harris Corporation for approximately $100,000. The size of the concentrator's diameter has been kept at 9 m as a "minimal" size limitation, because it provides a fade margin of 3dB. The demonstration will still yield a measurable amount of power with the fairly low incident densities.

The parabolic concentrator dish will reflect the incident 2.45 GHz waves with a 0.056 W/m^2 incident power onto a single dipole element, providing 2.69 watts of power at the focal point. Assuming that the polarization of the reflected power is aligned correctly with the dipole, the total system DC power output should be constrained to the efficiency of the rectenna placed there. Assuming an 80% efficiency, the output power is 2.15 watts.

Tracking

A tracking system is employed to manipulate the collector throughout the satellite pass. The tracking DC-SCU requires several predicted pass paths while in a "learn" mode to obtain consistent information. It then operates with the typical 2-D box signal tracking. This unit can also be purchased from Harris Corporation for approximately $40,000.

Additional tracking will also be necessary to maintain optimum polarization alignment of the linearly polarized 2.45 GHz wave onto the rectenna dipole. To implement this, there are several considerations. The first possibility is the use of a single foreplane rectenna. Essentially, this is two superimposed arrays oriented for perpendicular polarizations. Although this seems a very likely future consideration because of its high efficiencies, it is most effective at higher power densities.

The method employed for polarization tracking utilizes a cross-polar dipole to detect cross polar incident power. It then attempts to orient the rectenna dipole as a function of the cross-polar power. The dipole will therefore be placed on a rotatable mount and continually positioned so the 2.45 GHz power density incident on the cross-polar dipole is minimized. This does not assure that the co-polar power is maximized, but serves as an additional gain in efficiency.

Other Considerations

Beacon

The ground station sends a beacon to the satellite. This beacon is strictly one way, and is not to be misinterpreted with the communication link. The beacon is sent at a frequency of 4.9GHz, twice that of the power beaming signal. It is generated with stable oscillators to provide the cleanest possible phase and frequency signal for use as a guidance for PowerSat's phased array. This beacon will serve not only as a phase source for PowerSat's transmitter, but also as a switch. PowerSat requires the detection of this signal to beam.

Communication

The ground station has a communication link with the satellite about 80% of the time. Allowing ample time for any minor beaming preparations and adjustments. Prior to power beaming, the satellite requires a beaming code, in addition to receiving the beacon. This code is transmitted shortly before a pass to notify PowerSat that the ground station is ready to receive power. The beacon is a subservient power switch and gives a point of tracking reference. The beaming code is the master fuse.

TDRSS provides local data to the ground station with minimal delay. This will provide earth observers with the condition of many of PowerSat's subsystems, however the critical attitude control and subsystem adjustments is done by on-board processors.

Future Expandability

At this time the concentrator is not portable. One of this size tends to lose efficiency for every assembly. However, if a portable concentrator with greater than 70% efficiencies becomes available, ground sites could be placed in many parts of the world. In addition, a linear phase front reflector would assist in increasing the rectenna efficiency. Care would have to be taken to also ensure the concentrator maintains a respectively high efficiency.

The development of a dual polarized rectenna array would certainly assist the system's efficiency, however, with the current densities, significant power in the cross-polar signal is not anticipated.

PowerSat will support added ground sites. The present power consumption allows beaming to only one ground site per day. However this ground site can be selected to allow a reasonable presentation at various locations on the satellite's orbital path. The only access requirements are prior permission by the beaming code and a supplied transmission beacon. With some prior availability scheduling, PowerSat can provide numerous presentations or measurements at a wide range of ground sites.

On a global scale, PowerSat is only a demonstration of a space-based power source, energy collecting and storage in space, and selective tapping by Earth or orbital based receivers. Development of more efficient storage devices, directional beaming, and collectors, the space power source will provide abundant power to many parts of the world. With just a few satellites, full earth coverage can be obtained, providing energy to any location at any time.

LINK BUDGET

ATELLITE PARAMETERS	
requency (GHz)	2.45
ransmitted Power (Watts)	102400
ain of Transmitter Antenna dB)	53.82
eed Losses (dB)	0
IRP (dBw)	116.93

RANSMISSION PATH ARAMETERS	
ctual Satellite Distance (m)	835000.06
ree Space Loss (dB)	158.65
aseous Loss (dB)	0.3
et Losses (dB)	158.95

ARTH STATION RECEIVER ARAMETERS	
eceiver Antenna Gain (dB)	46.01
eed Losses (dB)	0
et Gain (dB)	46.01
ower Density on Ground W/m^2)	0.056
ower Received (dBw)	3.99
inimum Power Receivable dBw)	0.97
ower Density at ectenna(W/m^2)	2.68
ower Generated(W)	2.15

ADE MARGIN (dB)	3.0191500

Variables:

Power transmitted (Watts)	102400
Efficiency of trans antenna	0.5
Efficiency of receiv antenna	0.75
Area of trans antenna (m^2)	576
Diameter of rec antenna (m)	9
Frequency (GHz)	2.45
Orbital Height (m)	835000
Elevation angle	90
Efficiency of rectenna elem.	0.8
Passive Element Gain (dB)	13
Minimum Rectenna Oper. Power(W)	1

MICROWAVE EFFECTS

Energy Density Levels

Wireless Power Transmission is the transfer of energy through a medium. Several possible problems associated with WPT are related to atmospheric breakdown and radiation exposure. Below is a list of standards used for design and safety considerations.

Atmospheric Breakdown[6]
Sea Level
~1,000,000 Watts/cm^2

Worst Case (Low Pressure ~ 1 mm Hg)
4, 23, 400 Watts/cm^2 @ 1, 2.45, 10 GHz respectively

Former Soviet Government Standards[7]
Worker Exposure
0.01 mWatts/cm^2 for 1 Working Day
0.1 mWatts/cm^2 for 2 Hours
1.0 mWatts/cm^2 for 20 Minutes

General Population Continuous Exposure
0.001 mWatts/cm^2

United States Standard
OSHA Exposure Standard
10 mWatts/cm^2 for 6 Minutes

Impact of SPS

Investigation of whether or not the SPS operation leads to changes in the Earth's natural environment, and the impact of any such changes is an ongoing part of a feasibility study being conducted by the Department of Energy. Include in the study are the affects on telecommunications, airborne and space objects, and terrestrial objects.

Telecommunications
A principle concern is potential impact on the ionosphere and the possibility that communications within and through the ionosphere would be affected.

Lower ionospher heating has been ongoing using stations in Platteview and Arecibo. These stations deposit energy as heat in the lower ionosphere. Effects on communications passing through heated areas were evaluated using the Platteview site.[8]

Effects on VLF Systems: Negligible.
Effects on LF Systems: Negligible.
Effects on MF Systems: Negligible.

Study on Effects for Higher Frequencies
The experimental work done at the Platteville site does not extend to the upper ionosphere. Further testing is necessary to completely answer questions concerning effects.

Airborne/Space Objects
Organics
The effects of an SPS on migratory birds that pass through the beam is expected to be noticeable. Full understanding of the effects requires further study.

Satellites
Satellites in lower orbit is exposed to energy from the beam. Initial studies show that most systems currently being used would experience temporary interruptions of service while traversing the beam due to increased noise levels. Shielding of future satellites is also a current possibility for mitigating the effect of broadcast power on orbiting objects.

Airplanes
It is anticipated that no fly zones will remove this problem.

Preliminary review of studies of effects on airplanes show no conclusive effects on airplane electronics or passengers flying through a beam.

Terrestrial
An exclusion zone would be in effect for an area surrounding the rectenna that would protect people from exposure to harmful levels of microwave energy. The definition of harmful levels of exposure to radio frequency energy is still being debated.

SECTION 3 MISSION ANALYSIS

MICROWAVE/ORBITAL/LAUNCH

MISSION ANALYSIS

Mission analysis is the process of turning the mission statement into reality, and to justify selections as they are made along the way. The steps of the mission analysis and design process are shown in figure 3-1. Following these steps, the design team first established broad project objectives and constraints. These broad objectives and constraints were:

a) the satellite cost less than a global satellite, like the Hubble Space Telescope, limiting the budget to less than $800 million;
b) to prove the concept of solar power satellites using wireless power transmission with a quantity of power on the surface;
c) and finally, that the design remain practical.

These broad concepts flowed through the stages of mission analysis to provide the current goals. The goals of this mission are: the demonstration of the proof of concept for space to earth power beaming, the collection of data for comparison with power beaming theory, and the attempt to use new technologies to advance the studies in space research.

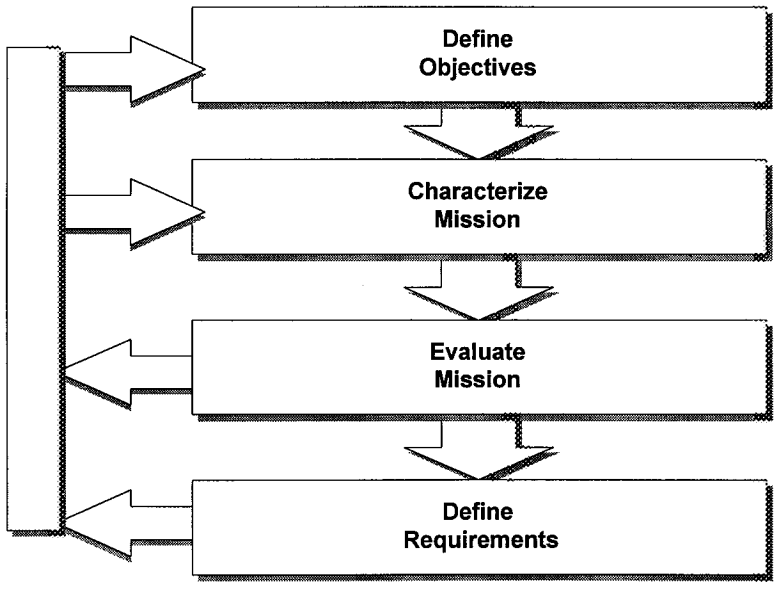

Figure 3-1 The space Mission Analysis and Design Process

The constraints of the project are:

a) the requirements of the experiment;
b) the cost;
c) the availability of developmental technology;
d) the demands of the space environment;
e) federal regulations;
f) and safety.

The optimization criteria are the ability to provide a functional system, and the reliability and utility of the system. The major necessary decisions are:

a) the choice of power density at the ground station;
b) frequency of power transmission;
c) amount of power transmitted size of the transmitting antenna;
d) and height of orbit.

Many of these factors involve trade-offs.

Cost Constraints

The cost constraint was based on initial estimates of sending high mass into a geosynchronous orbit. The initial budget was $800 million, but is now $100 million. This restraint is based on a future medium range power project, with support from the government, as a proof of concept for a power source. The project is limited mostly by cost when considering the possibility of implementation. The design team's goal is to produce the proof of concept for the lowest possible cost.

ORBIT SELECTION

PowerSat's orbital choice has to meet the mission's scalability, cost, and flexibility needs. The criteria for determining the orbit are flexible since different orbital parameters demonstrate different advantages and disadvantages. The primary criteria used for determining the PowerSat orbit are:

a) minimize free space lost in the system by choosing a low earth orbit;
b) maximize the pass time available for power beaming to a selected ground station;
c) maximize the satellite's total lifetime by choosing an altitude that reduces the satellite's drag forces.

A number of other factors affect orbit selection. Obviously the satellite has to pass over the selected ground station site daily to meet the second criterium. To minimize the payload weight, a low, or zero ellipse time orbit will reduce the number of required on-board batteries. Satisfying 100% of all the criteria, while maintaining the scope of the mission, is patently impossible. The process of orbital selection becomes one of the trade-offs between the various criteria and cost. These decisions

were made early in the design process and modified only as required. Figure 3-2 illustrates PowerSat's orbit.

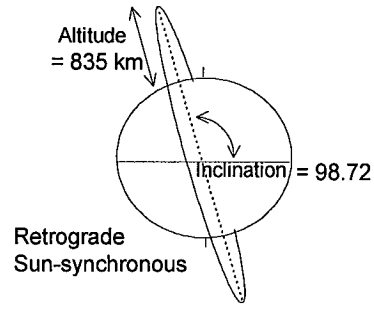

Figure 3-2 PowerSat Orbital Parameters

Orbital Parameters

A satellite's orbit around the Earth can be described in terms of six Keplerian elements that define its position to the Earth at any particular time. These Keplerian elements set the initial orbit conditions and define such factors as the satellite's speed, it's orientation with respect to Earth coordinates, and any orbit deformation. The classical Keplerian elements are:

- ***a:*** Semi-major axis is a measure of an orbit's size. For a circular orbit this is equal to the radius of the orbit.
- ***e:*** Eccentricity is the degree of the orbit's ellipsicity.
- ***i:*** Inclination is the angle between the orbital plane and the equator.
- **Ω:** Right ascension of ascending node is an initial condition which specifies the angle between the Vernal Equinox and the point where the satellite crosses the equator from south to north.
- **ω:** Argument of perigee is an initial condition that specifies the angular distance from the ascending node (where the satellite crosses the equator from south to north) around the orbit to the point of the satellite's perigee.
- ***v:*** True anomaly is the time elapsed since the satellite passed the point of perigee.

Since two of these elements, *right ascension of ascending node* and *true anomaly*, specify initial conditions, these two elements can be discounted by leaving the specification for insertion until later. These factors will only need to be calculated when setting the satellite launch time. This level of detail is beyond the scope of this preliminary design proposal, and need not be defined until a project time line and launch dates are proposed.

Two other elements, *eccentricity* and *argument of perigee*, have essentially no meaning for a circular orbit. If eccentricity were set to zero, then the argument of perigee could also be set to zero with no affect on the orbit itself. Consider the reason for a low eccentricity orbit by looking at the advantages normally gained with a high eccentricity orbit.

During a eccentric orbit, a satellite's velocity is lowest at its farthest point from the Earth. If the satellite's distance (altitude) from the cround station is not a significant factor, intentionally inserting a degree of eccentricity into an orbit gains pass time at apogee. However, PowerSat's altitude over the ground station is a major factor. Free space loss increases with the square of the distance. In order to achieve the lowest free space loss, PowerSat must be inserted into a low earth orbit; and since no gains are to be achieved by introducing eccentricity into the orbit, this value can be set to zero. PowerSat will have a circular, or near circular, orbit.

By process of elimination, the orbital selection for PowerSat can be defined by only two parameters: *inclination* and *semi-major axis*. A more intuitive way of defining the orbit is to express the orbit in inclination and altitude terms at zenith, since in circular orbit the altitude of a satellite overhead is the radius of its orbit, minus the radius of the Earth.

Altitude

Starting with the satellite's altitude, the orbital criteria must be considered. All three primary criteria impact the satellite's chosen altitude. Because free space loss worsens with altitude while time improves, the primary criteria implies trade-offs at various altitudes. The third primary criterium, establishing a usable satellite lifetime, sets the lower limit on the altitude, because the lifetime of the satellite is most severely affected by atmospheric drag at lower altitudes.

Between a 500 and 800 km altitude atmospheric drag on the satallite's cross-sectional area is a factor in establishing a three-year satellite lifetime. Above 800 km, the effects of atmospheric drag are subsumed by those of solar impingement. Rather than try to calculate the effects of drag on the surface of the array for an altitude between 500 and 800 km, the minimum orbital altitude was arbitrarily set to 800 km. For the sake of comparison, however, the pass time, gain and antenna size were calculated using these altitudes.

The satallite's optimum altitude is left to free space loss and pass time criteria. Comparing these values with each other demonstrates the effect of increasing the altitude, shown in figure 3-3.

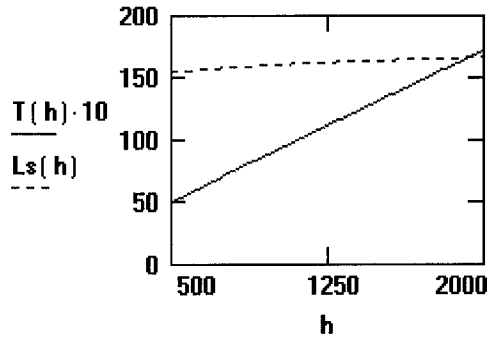

Figure 3-3 Comparison of Free Space Loss (Ls [dB]) and Satellite Pass Time (T [min. x 10])

Although the pass time increases significantly as the altitude increases, a minimum power density at the receiving sight must be obtained. Also, beaming a 100 kW signal from a higher altitude for significant time periods increases the requirements for solar panel size and storage capacity. In order to minimize the weight and size requirements for the satellite power systems, a pass time in the range of 5-10 minutes per day was accepted. This time amount is sufficient to conduct power beaming trials, yet conserve mass and volume in the power systems by reducing the solar collector's size and the number of batteries required.

Altitude thus becomes dependent on reducing the free space loss, acceptable minimum pass time, and an acceptable power density reception at the receiving site. Establishing 800 kilometers as the absolute lower limit, and factoring in the Taurus lift vehicle's insertion tolerances, places the orbital altitude range between 820 - 850 km. To expedite calculations, altitude is set at 835 kilometers.

Inclination

The final consideration for the satallite's orbital parameters is to set the satellite's optimum inclination. First, the satellite has to pass over the ground station in a near straight line to accommodate the phased array antenna's linear polarization. Second, this pass has to be regular, occurring at least once each day.

To guarantee that the satellite passes over the ground station at least once each day, either an integer posigrade orbit must be used, or some form of retrograde orbit. Any other orbit would experience some form of nodal precession, causing periods of several days where the satellite does not pass within the ground receiver site's power beaming range. Figure 3-4 illustrates how the precession would affect the viewing of the satellite for a noninteger posigrade orbit. As the node precesses, the ground station is left outside the satellite's effective coverage.

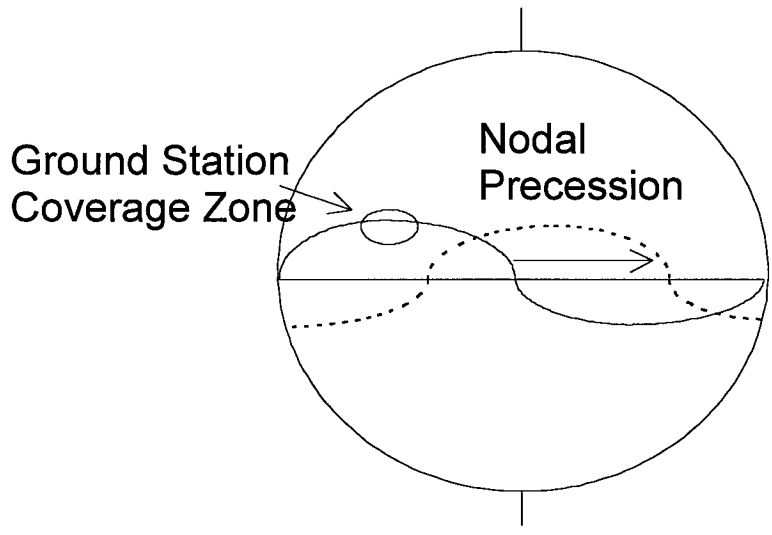

Figure 3-4 Example of Nodal Precession Affecting Ground Station - Satellite Viewing

An integer posigrade orbit must be set using the satellite's altitude to ensure that the number of passes is an integer. An 881 kilometer altitude, giving 14 satellite orbits and 13 apparent orbits per day, best fits the criteria. When the inclination is set approximately equal to the ground station latitude, one overhead pass per day for mid latitudes is established.

However, a better solution exists. By inserting the satellite into a retrograde orbit, a gain of at least two passes per day is realized for nearly all latitudes, regardless of an integer orbit. This retrograde orbit can be adjusted to allow the Earth's rotation to account for the satallite's apparent East-West motion while the satellite revolves about the Earth in a polar direction. In fact such an orbit may not necessarily be retrograde as long as it is a high inclination orbit.

An additional benefit is gained using a retrograde orbit. The satallite's angular velocity has two components. The first exists normal to the angular velocity of the Earth's revolution about the Sun. The second, is parallel to the angular velocity of the Earth's revolution. If the second component is set equal in magnitude to the angular velocity, but in the opposite direction, then the plane of the satellite's orbit will always have the same orientation with respect to the sun. This is known as a sun-synchronous orbit. This is shown in figure 3-5.

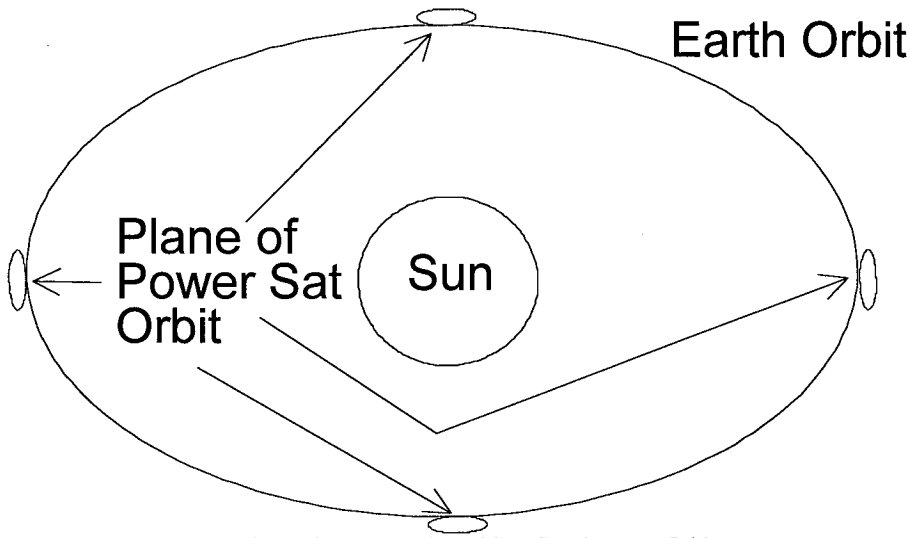

Figure 3-5 Illustration of Sun-Synchronous Orbit

By setting the argument of ascending node so that the satallite's orbital plane is normal to the sun, the satellite will always be illuminated by the sun. Since the solar panels will be continuously oriented toward the sun with limited movement required to maintain their positioning, an advantage is provided when developing the spacecraft power systems. Further, the satellite does not experience an eclipse in this orbit, thus requiring fewer batteries to maintain system power. The calculation of the solar impingement effects and thermal radiation are also simplified because only one aspect of the satellite need be considered. The advantages inherent in a sun-synchronous orbit makes it the optimum choice, provided it meets the pass time requirements.

Because the average angular velocity of the Earth's orbit is 0.9856 degrees per day, calculating a sun-synchronous orbit inclination becomes simple:

$$I = a\cos\left(4.77348 \cdot 10^{-15} \cdot \sqrt{R^7}\right) \qquad \text{(eqn 3-1)}$$

Where

I is the inclination for sun-synchronous orbit.
R is the Radius of the orbit = Altitude + 6378 kilometers

Solving this equation for the nominal altitude of 835 kilometers yields an inclination of 98.72 degrees.

Pass Time Calculations

With the orbit specified, a pass time for a given ground station can be calculated. By specifying a site's maximum pass time, the satallite's visibility time is calculated. To evaluate the ground station's expected performance, a computer orbit simulation can be use to predict visibility times.

The maximum pass time for the satellite may be found using the following formula:

$$T(h) = \frac{P(h)}{\pi} \cdot a\cos\left(\frac{\cos\left(\lambda_{max}(h)\right)}{\cos\left(\lambda_{min}\right)}\right) \qquad \text{(eqn. 3-A-2)}$$

Where

T is the satellite Pass Time [min.]
P is the orbit Period [min.]
λ_{max}, λ_{min} is maximum and minimum Earth ground station central angles with respect to the satellite (for PowerSat's array these are estimated at λ_{max} = 13.8° and λ_{min} = 0°)

A maximum of 7.82 minute pass time is calculated for the ground station. Interestingly, the maximum single pass time for a satellite in integer posigrade orbit at 850 kilometers is only 7.92 minutes. The difference in maximum pass times between the two orbits is only 6 seconds. However, the sun-synchronous orbit has two passes per day (one on the dawn-side of the Earth and the other at twilight for the proposed PowerSat orbit).

Though PowerSat passes the ground station twice each day, both passes are not optimum. A computer simulation modeled the satellite orbit with a cyclic pattern of long and short passes. However, there is either a dawn or twilight pass daily. The worst case scenario is two short passes with two minutes of total coverage. The best sce-

nario is both a long twilight and dawn pass, worth 15 minutes of total coverage. This is a significant advantage over a posigrade orbit that gets only one usable pass per day, unless the ground station is near the equator.

Since maneuvering JRTs would be detrimental to the large transmitting array, PowerSat employs no maneuvering capability. The only failure mode in orbital position is loss of altituor. Any other change in orbit position would result only in a variation of pass time, which is not critical; or in a loss of sun-synchronicity, which would affect only the solar array pointing (see section 4).

Loss of altitude affects the mission lifetime based on the atmospheric drag experienced at lower altitudes. Insertion at 800 km ensures that altitude loss will not be significant during the three-year design life.

Conclusion

By selecting a sun-synchronous orbit at 835 kilometers with a 98.72° inclination, significant advantages are gained in pass time, power system efficiency and flexibility. Though not mentioned previously, a mission flexibility by-product was discovered accidentally. The computer simulation determined that the actual longitude of the ground station did not have any impact on the pass time modeling, and latitudes between +/- 60° were also very similar in their pass time predictions. This gives the PowerSat project the capability of utilizing mobile sites for microwave wireless power transfer demonstrations at various worldwide locations. For latitudes above 60° N or S and below about 82°, the daily pass number dramatically increases to as many as four per day. The only limitation is the PowerSat's $100 million price cap. This budget limits battery capacity and total amount of energy that can be beamed in a given twenty-four hour period. However, with adequate coordination and scheduling PowerSat could be used on a global basis for propagation and wireless power transfer experiments.

LAUNCH SYSTEMS

Launch Vehicle Criteria

The launch vehicle selection depends on two concerns: the chosen orbit, and the mass size that is to be lifted to that orbit. As the mass of the payload and orbit altitude increase, so does the energy required to lift the payload to its fixed orbit. A third energy concern is the orbit inclination. Because of orbit inclination, the launch energy requirement increases with the launch site latitude. For the PowerSat proposal, the spacecraft orbit lies at 834 km, with a 98° inclination sun-synchronous polar orbit. The current total mass of the system is 603 kg. These numbers can then be used as the criteria to determine the launch vehicle needed.

The mass budget is table 3-1:

Table 3-1 Mass Budget

Description:	Mass (kg)	Mass % of Subsystem	Mass % of Total	%of Taurus Capability
Power System	293.2	100.000	48.648	39.093
Solar Panel	50	17.053	8.296	6.667
Batteries	200	68.213	33.184	26.667
High Voltage Switch	10	3.411	1.659	1.333
Low Voltage Switch	1.2	0.409	0.199	0.160
Transformers	32	10.914	5.309	4.267
Microwave	72	100.000	11.946	9.600
Magnetron	32	44.444	5.309	4.267
Phased Array Ant.	40	55.556	6.637	5.333
Attitude Control	44.1	100.000	7.317	5.880
Momentum Wheels	40	90.703	6.637	5.333
GPS	4.1	9.297	0.680	0.547
Housekeeping	193.4	100.000	32.089	25.787
Computer	11.4	5.895	1.891	1.520
Heat Tape	2	1.034	0.332	0.267
Structural	160.000	82.730	26.547	21.333
Communications	20	10.341	3.318	2.667
Mass Totals	603		100.000	80.360

Capability of Taurus: 750 kg

Application of Taurus Vehicle

The Taurus is designed for small to medium launch payloads, and presently fulfills PowerSat's application needs. With an ability to place up to 750 kg in the selected orbit, the Taurus can easily handle PowerSat's 600 kg mass budget.

The Taurus is manufactured by Orbital Sciences Corporation, which market the vehicle in three forms. The standard Taurus is currently in production at an estimated $30 million cost. The Taurus XL, currently being developed, will handle approximately an additional 100 kg capacity. The Taurus XL/S will also increase performance, but is only in its research phase. Figure 3-6 displays the performance characteristics of the Taurus vehicle.

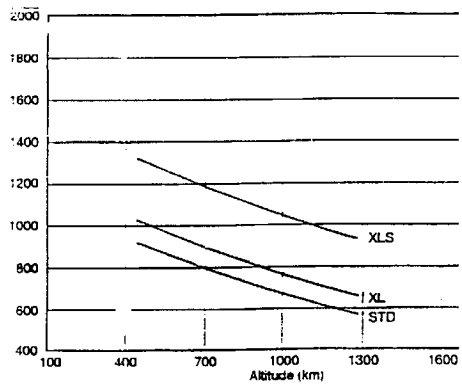

Figure 3-6 Taurus Performance Curves

Taurus Launch Vehicle Specifics

The Taurus was first developed under the supervision of the Defense Advanced Research Projects Agency (DARPA). Orbital Sciences Corporation (OSC), a DARPA child, took over the Taurus and Pegasus programs. The Pegasus, a winged, airborne launched, capacity vehicle, took its first flight in 1988. Taurus is OSC's next step beyond Pegasus, incorporating much of the same hardware. Taurus' special attribute is a five-day launch set-up time on any unimproved concrete pad.

The standard Taurus is a four-stage solid propellant vehicle. A simple picture of the Taurus is shown in figure 3-7.

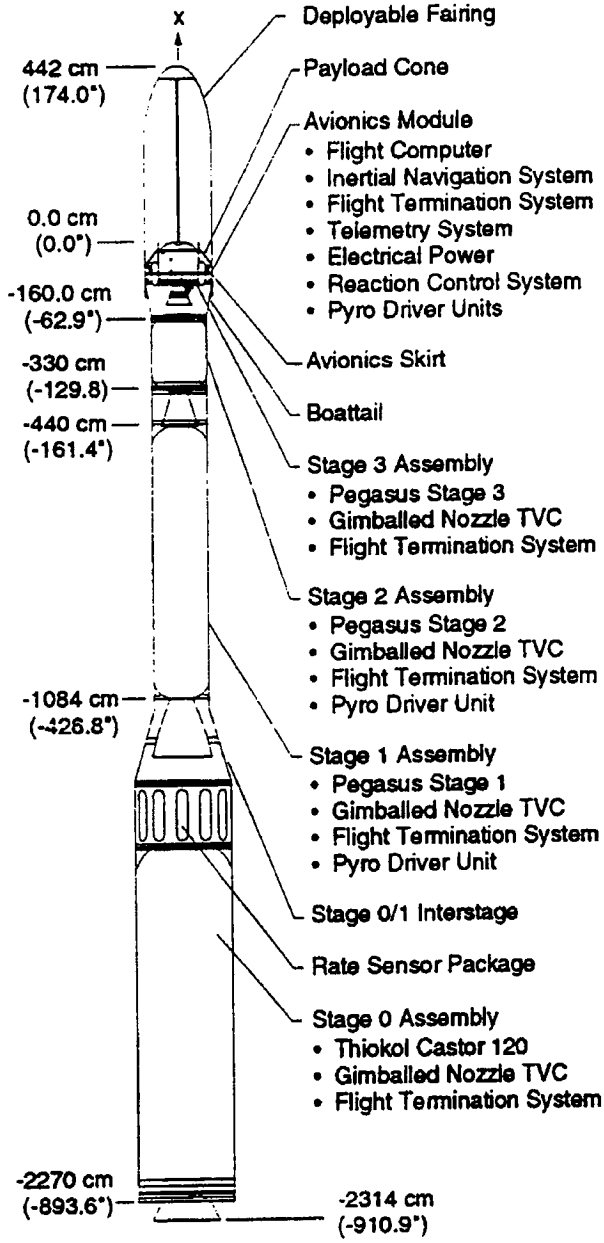

Figure 3-7 The Taurus Vehicle

A complete set of transportable launch support equipment (LSE), is included with the Taurus. This equipment is designed to make the Taurus an independent satellite delivery system. A graphic representation of the complete launch system is shown in figure 3-8.

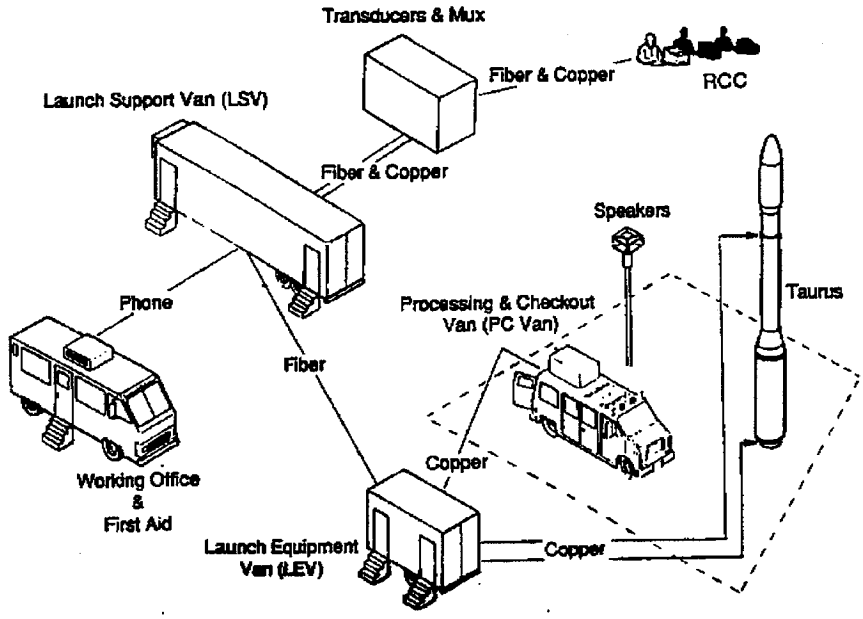

Figure 3-8 LSE Transportable Launch Support Equipment

Within the LSE is a launch stand, the Launch Equipment Van (LEV), the Launch Support Van (LSV), and assorted equipment necessary for a launch. The LSV is the launch central control center, and includes OSC, range safety, and payload personnel. The LEV carries the majority of the equipment for the launch. The Taurus is capable of autonomous operation, but the LSE is compatible with launch facilities at the Air Force's western and eastern ranges. The LSV is connected to Range Operations Control Center.

As stated before, the Taurus is a four-stage solid propellant vehicle. When OSC adopted the Taurus program from DARPA, they kept the top three motors: the Hercules Orion 50s, Orion 50 and Orion 38, but changed the bottom booster to the Peacekeeper's Thiokol Castor 120 motor.

The Taurus motor nomenclature is slightly unstandard. All three Hercules motors comprise the Pegasus launch vehicle. In order to keep the naming of the motors the same, Taurus' second stage motor (first stage on the Pegasus) is called the first stage. Taurus' first booster is therefore called the "zeroth" stage.

In order to launch, the Taurus requires a 40 ft x 40 ft concrete launch pad suitable to support the Taurus launch stand. All other equipment and buildings around the launch are not mandatory, but can be used if needed. The LEV houses the power supply, computers, and other equipment needed in close proximity to the launch pad.

The LEV also houses payload specific devices such as battery chargers. The LSV controls the launch through a fiber optic cable connected to the LEV. The LSV holds the payload personnel and the devices needed to monitor the payload during launch.

Taurus Performance

Once the Taurus system is ordered, OSC customizes the launch path to fit the payload's needs. There are two types of trajectories used to put the payload into orbit: a direct ascent (which is used for LEO orbits), and a parking orbit ascent (generally used for transfer orbits). PowerSat is placed into orbit using a direct ascent launch. A graphic summary of the launch is in figure 3-10.

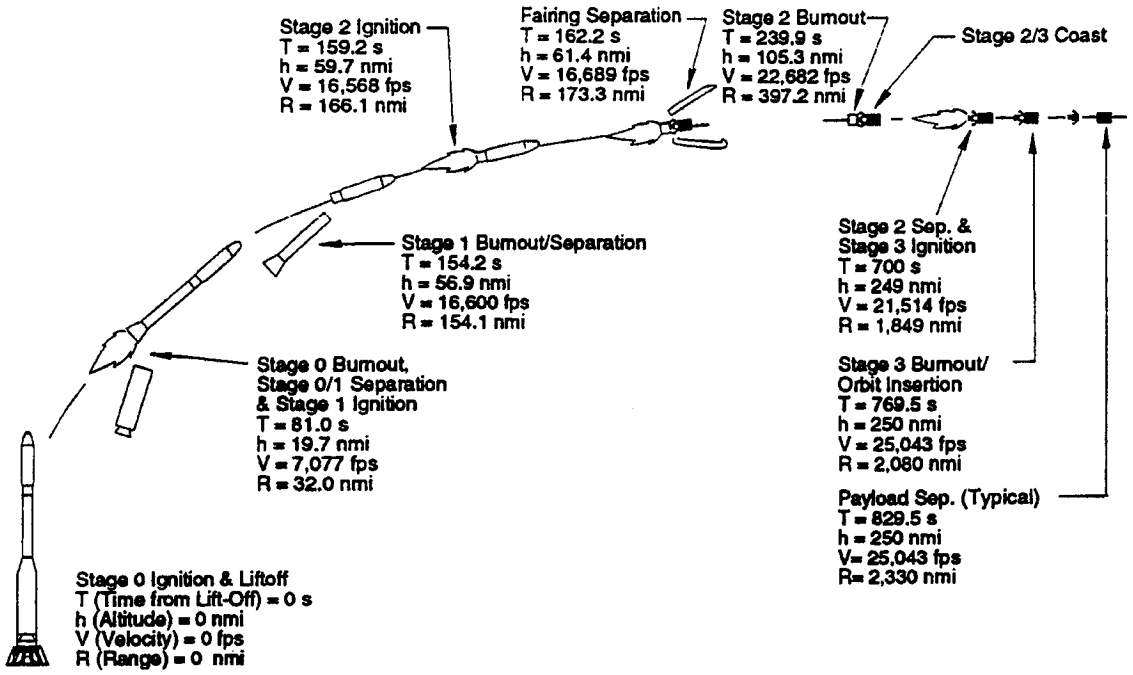

Figure 3-10 Direct Ascent Launch

Increased Performance Options

Orbital Sciences Corporation is planning production of two other Taurus vehicles that will increase performance. Both vehicles are designed to use currently available additions, making them much more reliable. The Taurus XL modifies the stage one and two boosters to allow for more propellant. These two longer boosters are the Hercules Orion 50S/XL and Orion 50/XL. Both of these motors are flight proven and highly reliable. The Taurus XL/S is currently a paper study to substantially increase the Taurus performance. The XL/S will use two additional Hercules graphite/epoxy motors strapped onto the Taurus XL. These strap on motors are used on the Delta II launch vehicle. The graphical comparison of the DARPA Taurus, OSC's Taurus, Taurus XL, and Taurus XL/S is shown in figure 3-11.

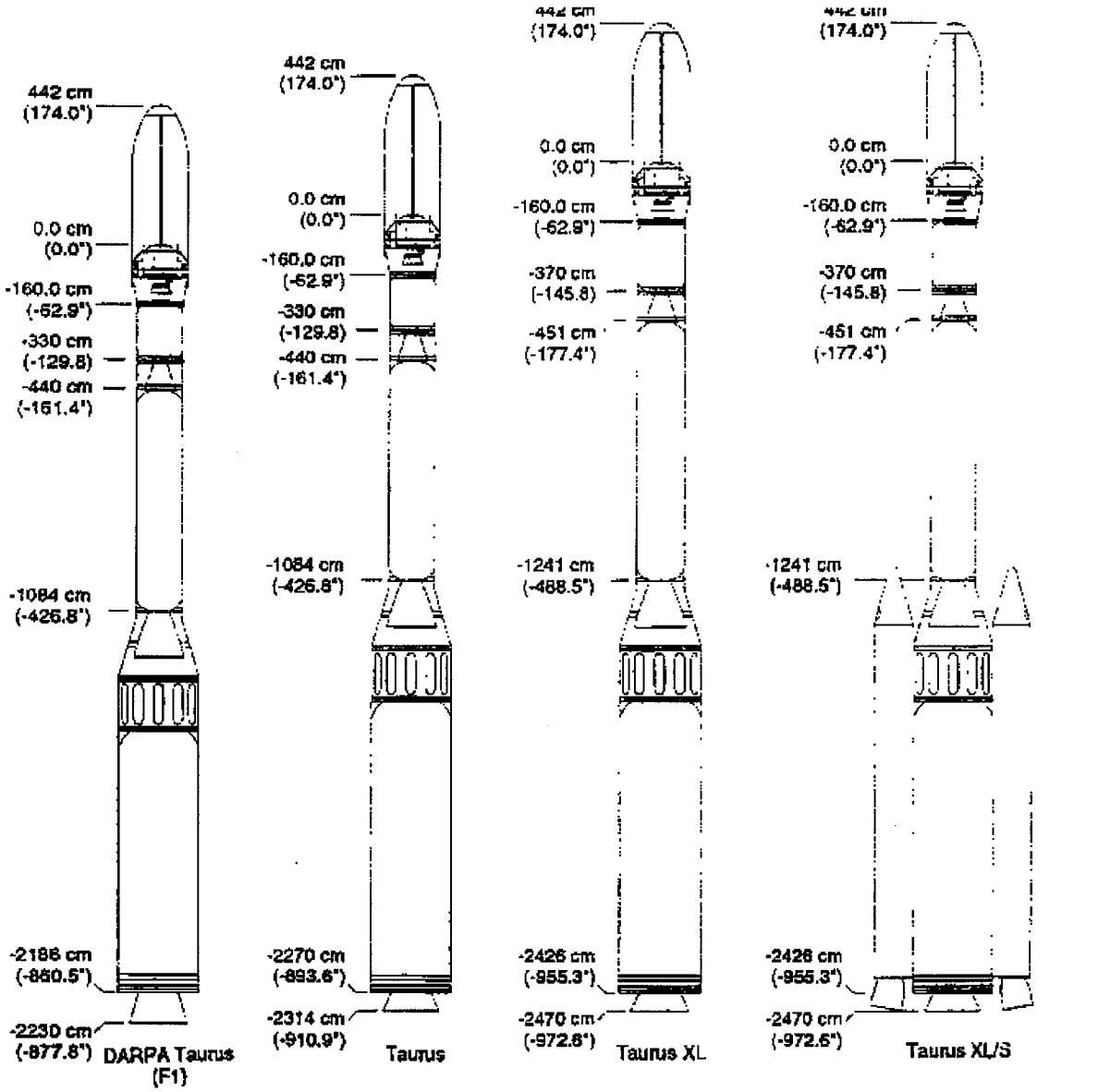

Figure 3-11

PowerSat will be launched using the standard Taurus, but if an unexpected change is made, Taurus' flexibility will accommodate more mass.

Payload Constraints

The major implication of the launch vehicle on the payload itself is the payload fairing's shape and size. All payload components must be stowed within the fairing. The profile of the fairing, with dimensions, is shown in figure 3-12. If the PowerSat payload mass were suddenly to change, thus requiring a Taurus XL or Taurus XL/S, the same dimensions will apply.

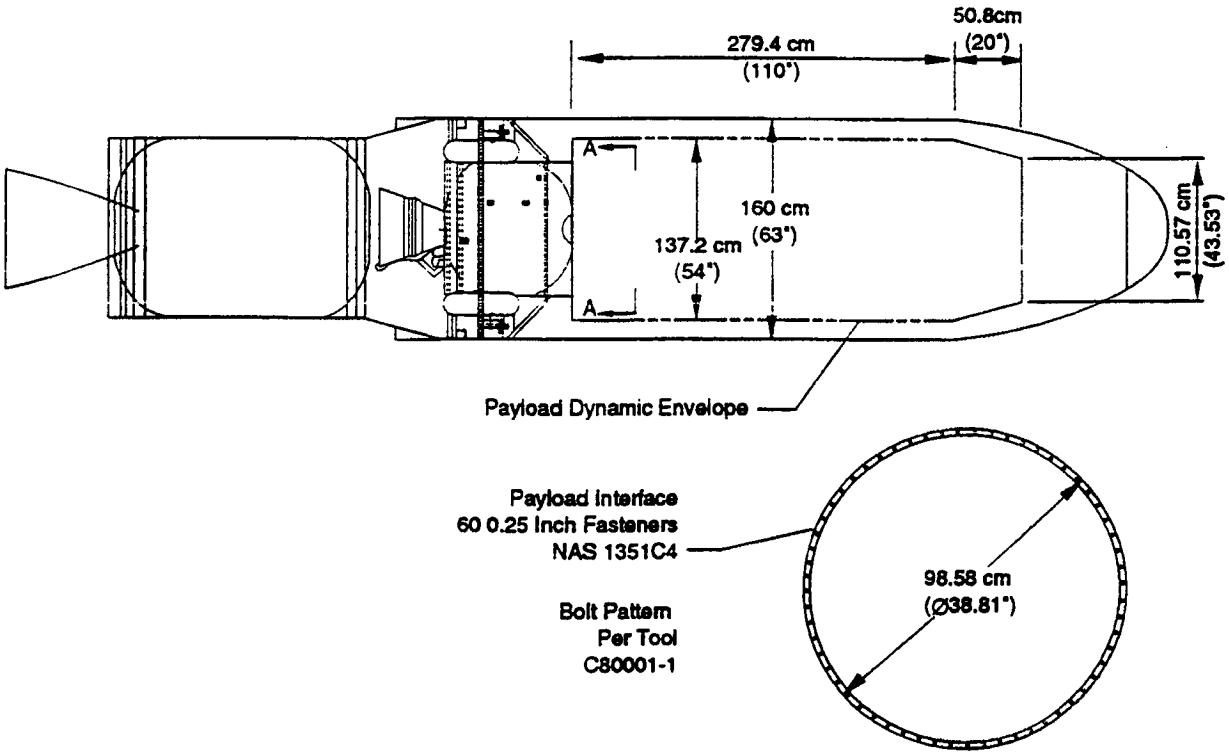

Figure 3-12 Taurus Payload Fairing Profile

SECTION 4 SPACECRAFT

SPACE DESIGN CONSIDERATIONS and SPECIFICATIONS

GENERAL CONFIGURATIONS

Phased Array Antenna

The phased array antenna is an inflatable structure 32 meters long by 18 meters wide in its deployed configuration. Preliminary specifications for this design were completed with assistance from Tracor Incorporated, an independent design firm specializing in rigid inflatable structures. The proposed flat planar array has a peak broadside gain of 66.8 dB for a 50% assumed antenna efficiency. The array is composed of 16 subarrays arranged in two rows of eight subarrays each. Each subarray is fed by two phase matched magnetrons, which in turn are fed by a low-power ferrite phase shifter. This gives the array a limited capability to electronically steer the resultant beam by independently altering the phase of the 16 separate subarrays. Figure 4-1 illustrates how this signal flow works, not shown is the signal provided to the phased shifters by the beacon.

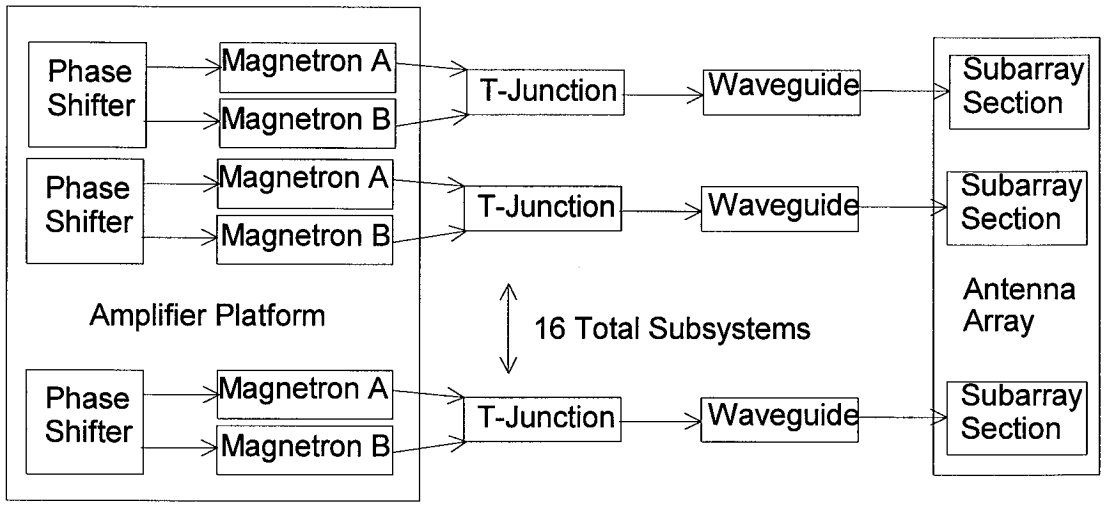

Figure 4-1 Signal Flow Diagram for Phased Array Antenna

Slot Element Specifications

The individual slot elements are the array's basic building blocks. These slots are configured crosswise in the feed waveguide and are 1/2 wavelength long (approximately 6.12 cm). In order to increase the gain of the array, Yagi-Uda

passive directors are added across the slot element. Each Yagi-Uda director is an approximately 5.82 cm long piece of 5 mil thick crimped titanium foil. The directors are then spaced approximately 1/4 wavelength (3.06 cm) apart. Adding these directories yields a nominal 13 dB of directivity to each of the slot elements, yielding an additional 13 dB to the entire array. The 13 dB is only a nominal value for the gain which may be achieved using the Yagi-Uda directors. Theoretically gains of up to 26 dB are achievable. This additional gain requires that the directors be optimized for each slot, including the mutual coupling effect of adjacent slots, and accounting for the phase differences between subarray sections. This may be accomplished using numerical methods and adequate computer resources, however this is beyond the scope of this design proposal. Whether this optimization is actually required for this project may also be debated since the nominal 13 dB of directivity is adequate for the mission proposal. The orientation of the directors with respect to the slot is shown in figure 4-2.

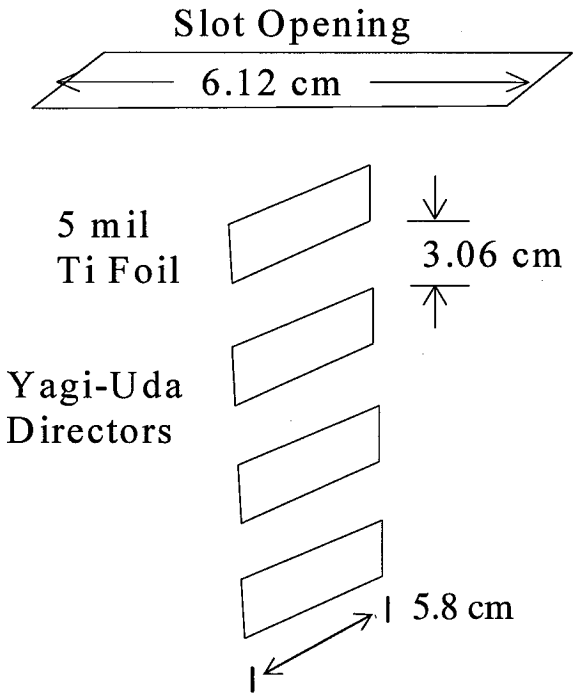

Figure 4-2 Slot Array to Passive Directors Alignment

Subarray Specifications

The 16 subarrays themselves are made up of 2190 individual slot elements arranged in what resembles a flag (figure 4-3). By using an inflatable structure the design must include the waveguide as part of the rigidizing structure. This is done by arranging the subarray as a series of 73 adjacent cylindrical waveguides. The waveguides are made of aluminum and mylar so that when the array is inflated, the aluminum is stretched to its maximum tensile strength. When the inflating gas is vented, the rigidized aluminum remains

formed. Naturally, this method is highly effective for large hollow structures, like this array, in a microgravity environment.

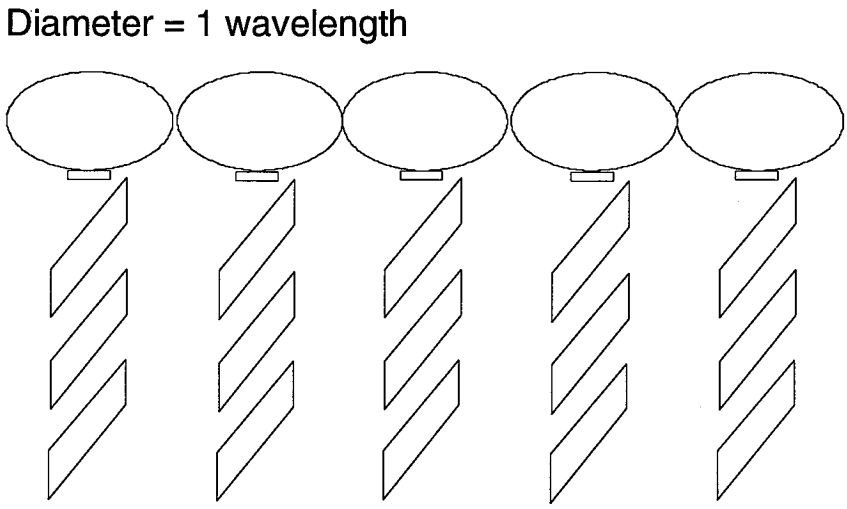

Figure 4-3 Subarray Section Showing Waveguide Structure

Figure 4-4 illustrates how the waveguide itself makes up part of the array's structure. Each subarray has a total of 73 waveguides that span the width of the section. These waveguides are fed from one end, giving the subarray its flag-like appearance. Care in the final design will need to be taken when calculating the actual waveguide diameter to ensure impedance matching within the subarray. Because the array will also be used to receive a low-level pilot signal, reflection of the outgoing transmission must be minimized. Using this design, the subarray can be fed from a single point at one corner.

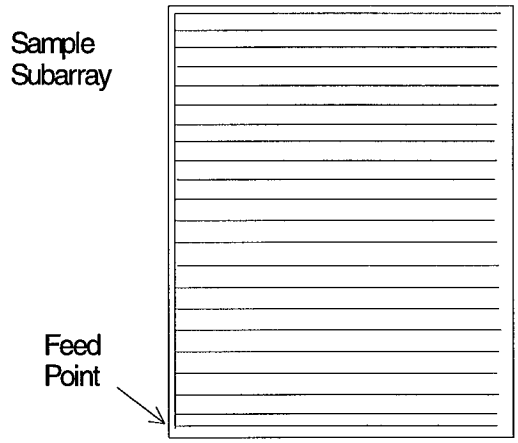

Figure 4-4 Representative Subarray Showing Flag-like Arrangement of Waveguide

Another concern when specifying the final design of the subarray is spacing of the slot elements. While the lateral distance between elements is determined by the diameter of the waveguide, and the distance between elements

on a single waveguide is easily set at ½ wave length guide, it is necessary to ensure that all elements on the subarray elements are in phase with each other. This can be done by specifying the location of the first element from the main feed and ensuring that all other elements are spaced an integer number of wavelengths away through the wave guide.

Array Specifications

The overall design of the array then is the combining of the 16 separate subarrays (figure 4-5). The total structure is 32 meters long and 18 meters wide. The total number of individual slot elements on the array itself is 35,040. The number of slot elements is well above the threshold required to consider this a uniform flat planar array. The feed point on this array is designed to be midway along one edge of the long axis. This is the point where the satellite itself will be connected to the array. Since a sun-synchronous orbit is used, this will also be the side which receives all of the impinging solar radiation. By making this the feed point, and running the 16 feeding waveguide along this edge, the structural strength of this edge is increased, and the effects of heat deformation are reduced.

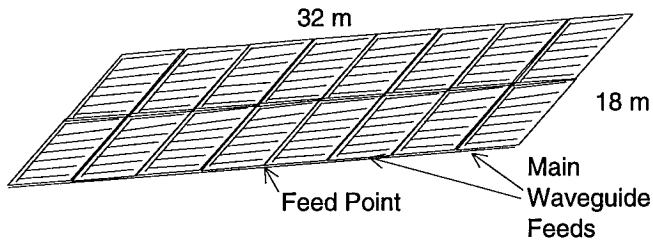

Figure 4-5 Complete Array Structure

Feasibility Study

The design for the inflatable planar array was coordinated with Rhonda Foster of Tracor, Incorporated and Tracor design team members, specialists in inflatable structures for space. They were able to provide significant help in researching the feasibility of this design. Based on sketches provided to them by the USRA design team, they were able to provide some specifics on the feasibility of the design. Tracor was able to verify that PowerSat's design presented no particular problem, and that the design would be structurally sound. Developing the feed and array arrangement requires some significant engineering, but is within the capabilities of their expertise, or that of a dedicated university design team. Based on Tracor's assessment, an initial cost estimate for the engineering, testing, and production of the array is between $10-15 million. This estimate is arrived at by the USRA design team, since the exact specifications are not available for Tracor to develop a complete cost estimate. Tracor did verify that the majority of the cost would be incurred in the design and testing of the array, and that the cost of constructing the array itself was relatively low. This would substantially reduce the cost of any following missions using the same design.

Since the array represents a singular point of failure for the experiment, a significant portion of the required engineering is in array failure analysis.

Future Considerations

By choice, no attempt was made in this analysis to investigate the exact transmission patterns for the array. Instead, all calculations used for attitude determination and gain calculations were done assuming that the subarrays could be modeled as individual uniform planar arrays. From this assumption, the performance of the total array could be modeled as a set of 16 planar arrays, with only the quantization levels of the subarrays affecting the transmission and gain equations.

Part of the required design process is to investigate the array's total performance to develop accurate transmission patterns, total gain, and steerability functions. This is considered beyond the scope of the USRA proposal, but is an integral part of the performance evaluation for microwave wireless power beaming, since the array performance has a major impact on the PowerSat project's efficiency calculations.

Photovoltaics

PowerSat uses photovoltiac solar cells to collect solar energy and convert it to electrical power.

In general, photovoltiac power conversion is accomplished in a cell fabricated with a thin pn junction between the outer layer and the substrate. This junction has the same affect as a permanent electric field. The impinging solar photons knock electrical charges from the solar cell's crystal outer shell structure. The positive charges are then directed into the p-type material by the pn junction field, while negative charges are directed to the n-type material. These charges form a usable current.

Prairies uses Gallium Arsenide cells on a Germanium substrate (GaAs/Ge). They are state-of-the-art cells with 18.5% power conversion efficiency.

Figure 4-6 shows the characteristic curve of these cells. Note that this is a constant current source out to 0.8 volts. If the load is an open circuit, the voltage applied to it is about 1.02 volts per cell in full sunlight. The point at which the cells deliver maximum power is slightly to the right of the curve's knee, or 0.89 volts. If the cells are loaded at this point, the power output is 24.8 me/cm^2.

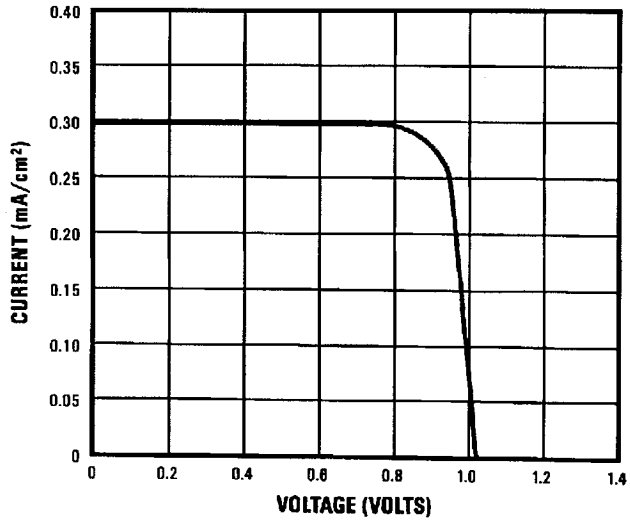

***AMO Sunlight (135.3 mw/cm²), 28°C**

Jsc = 29.6 Milliamperes/cm²
Jmp = 27.8 Milliamperes/cm²
Vmp = 0.890 Volts
Pmp = 24.8 Milliwatts/cm²
Voc = 1.020 Volts
Cff = 0.82
Efficiency 18.3% Minimum Average
***AMO Sunlight (135.3 mw/cm²), 28°C**

Figure 4-6

With the voltage-to-current characteristics shown, the most efficient way to use these cells is to arrange the cell stack voltage to be slightly higher than the battery float voltage, then simply bridge the panel output (through pass diodes) across the batteries.

Charge regulators are set up to short the panel output to ground if the battery voltage gets high enough to cause damage, but this does not occur under normal conditions.

SPACECRAFT STRUCTURE AND CONFIGURATION

Launch Vehicle Constraints

After evaluating the mission requirements, the Taurus launch vehicle manufactured by the Orbital Sciences Corporation was selected for orbit delivery.

This dictates the maximum mass and stowed volume that can be placed at our specified sun-synchronous orbit. Figure 4-7 shows the Payload envelope for the Taurus Launch vehicle.

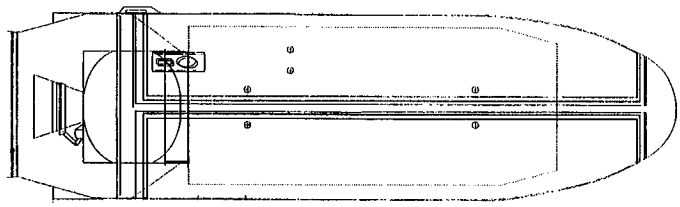

Figure 4-7 Taurus Payload Fairing

The launch environment provides the worst case loads that the spacecraft will experience during the projected mission lifetime. This dictates the maximum quasi-static gravitational loadings, vibration loadings, and shock loadings. The peak design loading on the spacecraft are listed in table 4-1.

Table 4-1 Launch Vehicle Induced Loadings

Mission Segment	X g's	Y g's	Z g's	Shock
Ground Operations	1.5	1.7	1.7	0
Flight Operations	9	0.5	0.5	4000g @ 1000-10000 Hz
On-Orbit Operations	0.02	0.02	0.02	0

Spacecraft Design

Deployed Configuration Design

The basic deployed configuration is determined by the solar array and inflatable phased array's specific requirements. Due to the selected sun-synchronous orbit, the solar arrays are positioned perpendicular to the incident sunlight.

The placement of the phased array, based on recommendations from Tracor, minimizes the overall disturbance torque's on the spacecraft. The resulting configuration is shown in figure 4-8.

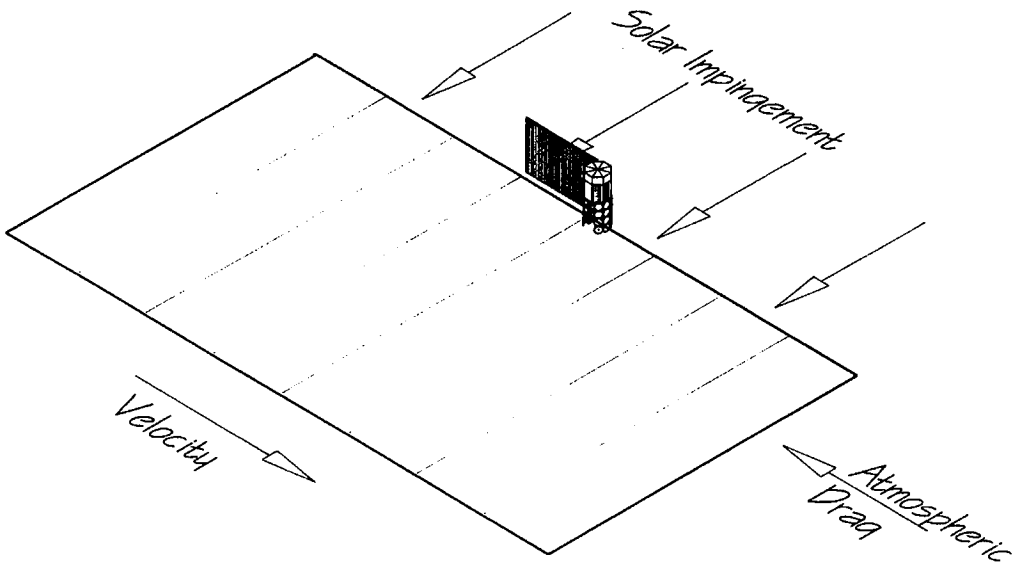

Figure 4-8 Deployed Spacecraft Configuration

Figure of Deployed Configuration

In order to find the maximum disturbance torque's that the spacecraft will experience in Earth's orbital environment, four disturbance torque's sources are considered. They are indicted in table 4-2.

Table 4-2 Summary Disturbance Torques

Source of Disturbance	Solar Radiation	Gravity Gradient	Aerodynamic
Max Torque - NM	$3.893X10^{-5}$	$5.23X10^{-7}$	$1.2X10^{-15}$

Structural Design

The material selected for the structural components is 7075 Aluminum. This material is selected on the basis of reliability, ease in manufacturing, good compatibility to the orbit environment, and excellent structural properties.

Table 4-3 Properties of 7075-T6 Aluminum

Material	Density lb/in^3	E MSI	UTS KSI	YS KSI	Design stress KSI	Cost $/lb
Aluminum 7075-T6	0.098	10.9	75	65	37	2

Typical spacecraft structures are between 20-25% of the overall spacecraft mass. Some of the more critical design issues that pertain to the launch loads are: sufficient rigidity to avoid resonance, sufficient strength, and that the displacement under loading on the structure does not violate the payload dynamic envelope during launch.

The design is based on the dimensions of the payload dynamic envelope for the Taurus booster as shown in figure 4-7.

The structure is an eight sided monocoque, structure using 0.10 in thick 7075-T6 Aluminum panels.

The solar array is wrapped around the perimeter of the payload structure. This configuration reduces the maximum size allowed for the payload structure. In order to provide sufficient flat surfaces for increased mounting reliability and storage capacity, an octagonal structure is specified. Preliminary sizing for both monocoque and stringer type structures was done, and a monocoque was selected to provide optimal rigidity.

The structure was optimized using the Finite Element Analysis Program, Cosmos\M. In each design iteration the natural frequency, moment of inertias, mass, and the high and low-stress regions were found, and the design was modified accordingly. The resulting structure is shown in figure 4-9.

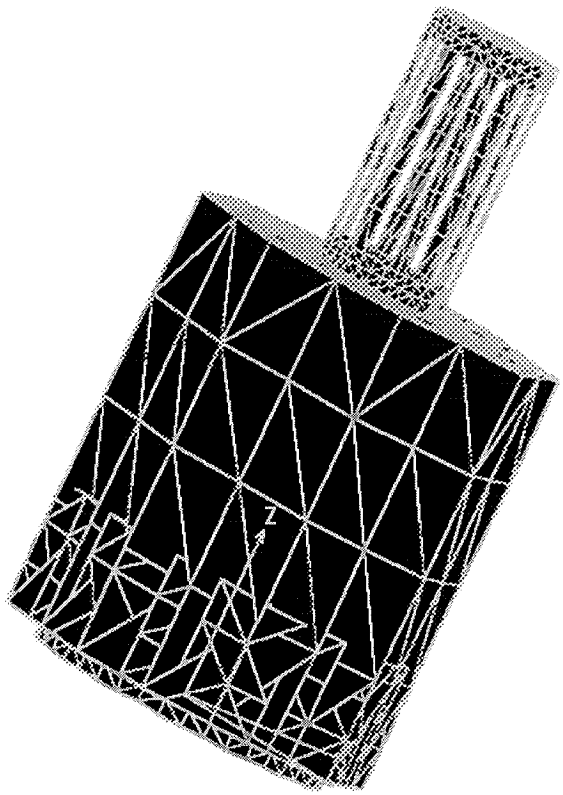

Figure 4-9 Structural Plot

The final structural design is 143 kg, approximately 19.7% of the overall mass of the spacecraft, and has a peak stress of 9800 psi, well below the shear yield stress of 37,000 psi for 7075 Aluminum.

Configuration Stowed

The payload layout is determined by the deployment method for the inflatable phased array and the environmental conditions optimal for the operation of each component. The octagon payload structure is split by two horizontal shelves, as shown in figure 4-10.

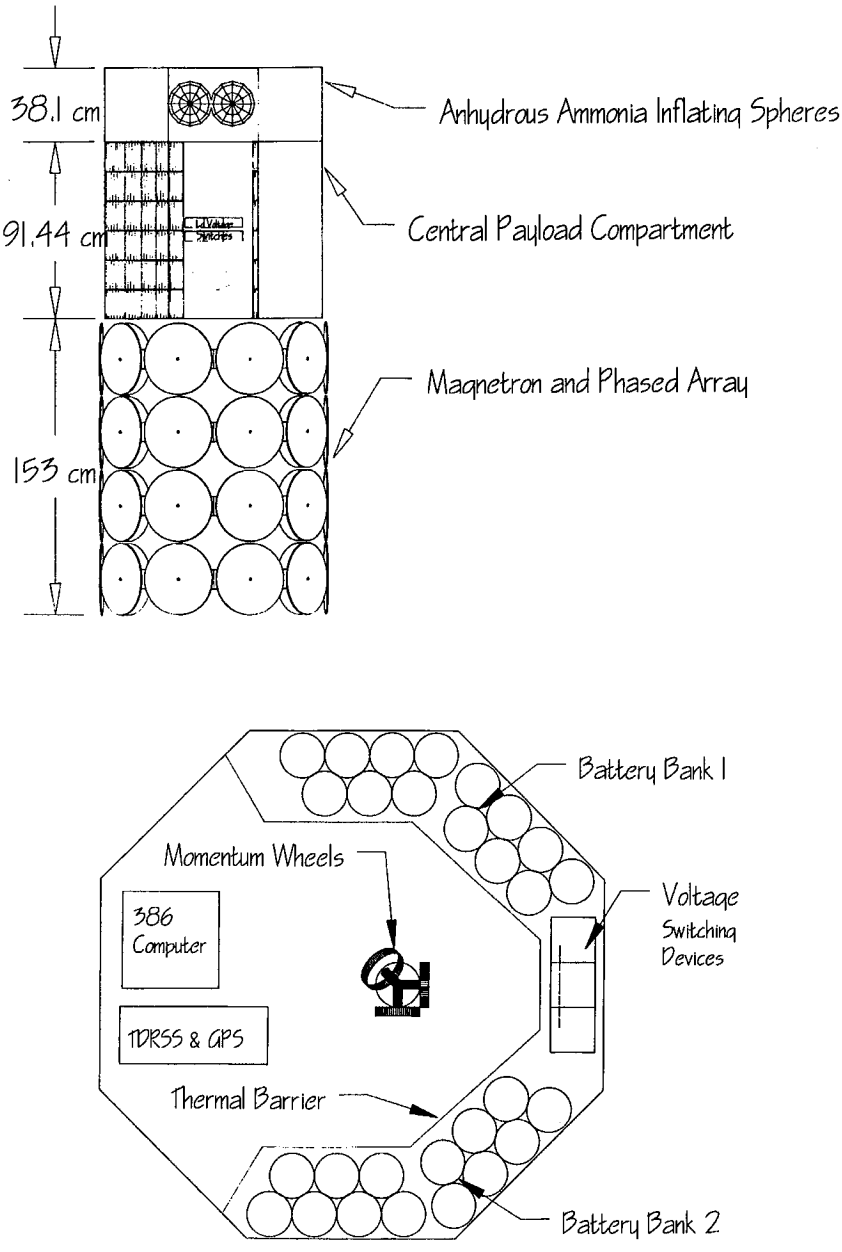

Figure 4-10 Stowed Configuration Picture

The lower compartment houses the communications antenna and the attitude control system sensors. This section is directly connected to the booster interface. The communications antenna, attitude control sensors, and a laser for controlling the phased array, are located in the section connected to the booster interface.

The middle section, the central payload module, is separated from the lower module by a shelf 15 inches above the payload interface plane. This section houses the momentum wheels, attitude control system, main computer system, batteries and power conditioning devices. This section is divided by a vertical radiator wall because of thermal considerations.

The top section contains the entire phased array deployment devices. This section is separated by the center module, and by a horizontal shelf 36 inches above shelf number one. This section is left uncovered, and has a central support structure for the magnetron devices, as shown in figure 4-11.

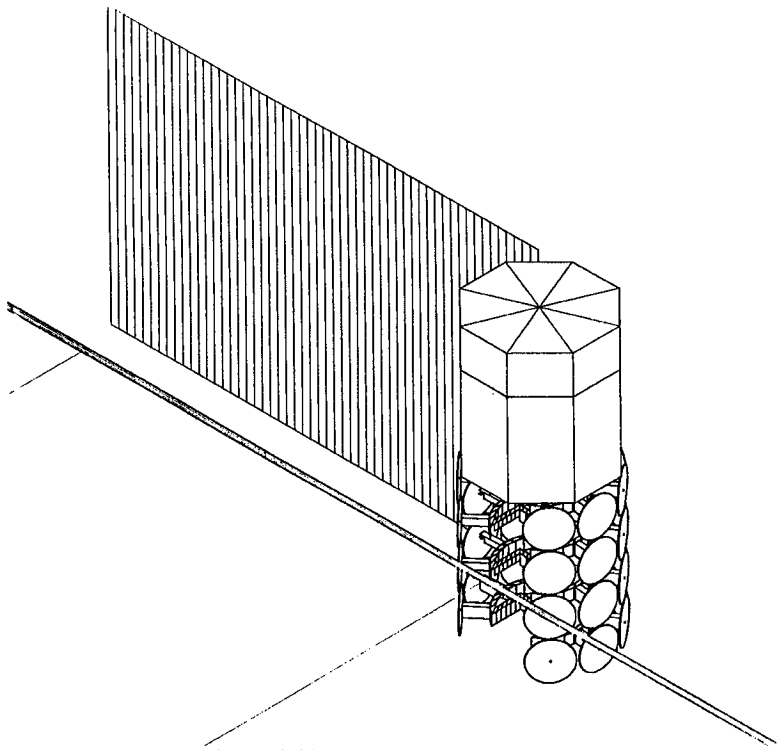

Figure 4-11 Deployed Payload Structure

Deployment

Payload Separation and Ordinance Devices

As previously mentioned, the launch vehicle consists of three stages. The payload fairing is jettisoned directly after the second stage burnout, and when the fairing dynamic pressure is 0.005 LB/ft^2. The maximum predicted shock input occurs from the payload fairing separation.

The third and final stage of the launch vehicle, ejects the payload approximately 30 seconds after burnout. Deployment is controlled by the Taurus avionics module. It activates the bolt cutters in the payload separation ring as shown in figure 4-12.

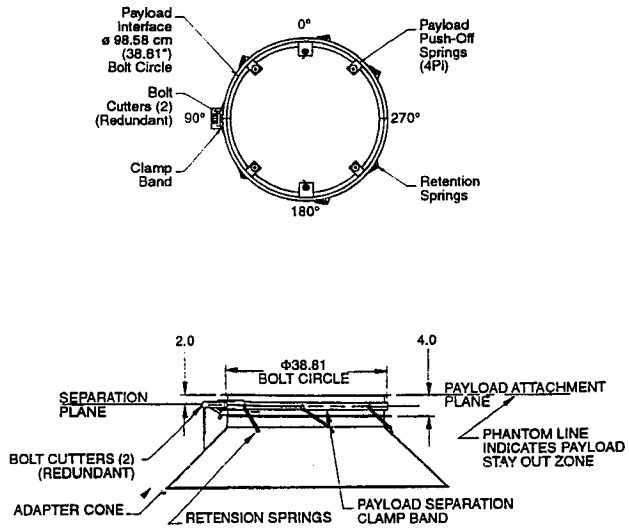

Figure 4-12 Taurus Separation Ring

Once the payload has been placed in orbit, the solar arrays and the phased array are deployed. The flexible solar arrays are lined by inflatable tubing along the perimeter. The tubing consists of an aluminized mylar, and is inflated above its yield stress by anhydrous ammonia.

The phased array skin consists of two layers: one layer of 0.2 mil mylar film covered with a second layer of 0.3 mil 2024 aluminum coating. Once inflated, the structure is about 9.15 cm thick.

The packaged phased array has a volume of 1.5 ft^3. The inflating, anhydrous ammonia, will be contained in a separate 9 inch diameter spherical tank. The entire inflation process takes approximately 20 ms.

ELECTRICAL POWER REQUIREMENTS

The power system chosen consists of a sufficient photovoltaic solar cell area to collect the required power over the course of the day. The solar tracking is on a single axis to optimize the angle of the panels. Batteries store power, and provide it to the on-board electronics. Both the panel and battery power will receive electronic conditioning. This system is shown graphically in figure 4-13.

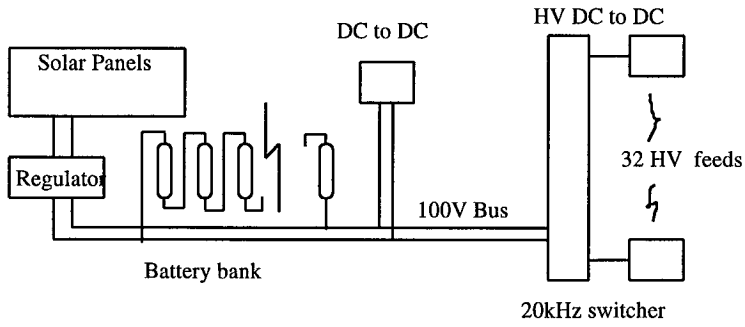

Figure 4-13 The Power System

Due to the short duration and high energy consumption during a pass, there is no attempt to supply a significant part of the transmitter experiment with direct solar cell power.

Power Demand

The spacecraft's demand for electrical power is given in table 4-4. The power requirements are of two types: a continuous, low-voltage demand, and the short duration high voltage needs.

The low-voltage demand is needed to power all of the spacecraft's systems, excluding the magnetron transmitters. It comes from a 100 volt bus using commercial DC to DC converters.

The batteries do not supply this power because the solar cells will continuously generate more than enough to satisfy requirements. Because it is continuously needed, this load is the greater portion of the power requirement.

The second load category is the high voltage used to power the transmitter magnetron tubes. This voltage is the one that presents the most trouble. PowerSat accumulates energy from the solar panels over the course of the day, stores it in a battery bank, then supplies it to the load in one large burst at over 120,000 watts for an eight-minute period each day.

Power Storage

The batteries chosen are state-of-the-art nickel-hydrogen cells with an improved nickel electrode. These cells are custom made. The new electrode is designed by Doris Britton at NASA Lewis. Commercial manufacturing is possible.

The published power storage density for nickel-hydrogen is 49 Watt*hours/kg. The new electrodes are said to double this. A conservative value of 91 Watt*hours/kg is used in these calculations, even though the data from NASA Lewis shows a somewhat higher figure.

The battery load is only used during a single daily eight-minute pass. The

32-magnetron power requirements, each needing 4500 volts at 0.8366 amps, is 120.5 kw.

To deliver 120.5 kw for eight minutes, 16 kW*hr storage is required. Allowing for a 72% discharge depth, and a 85% battery/converter efficiency, PowerSat needs 27 kW*hr. The above-mentioned 91 Watt*hr/kg has a 291 kg battery mass.

The batteries are most efficient at around zero degrees Celsius. They operate adequately between -10 to +20°. They generate heat due to internal resistance, and have a conversion efficiency of about 85%, with most of the loss appearing as waste heat. A passive cooling scheme is designed to prevent the battery temperature from rising above this range.

The cost of such a system will be about $100,000/kW*h, totalling $2.7 million.

Power Generation

Equation 4-1 is the formula used to determine the required solar panel surface area.

$$P = P_s * A_{sp} * Eff * Cos(SA) \qquad \text{(eqn.4-1)}$$

where

A_{sp} is the Area of the solar panels in m^2
P_s is the Power density in W/m^2
Eff is the Cell efficiency
SA is the Angle at which the incident solar energy strikes the panels
P is the Power generated

This gives the instantaneous power collected, but the energy amount collected over the course of a 24-hour period is desired. Because the angle of the panels to the sun is constant, and the panels are kept at optimum angle by using a single axis drive motor, and the geometry of the spacecraft design, the accumulated energy becomes:

$$P = 24*P_s*A_{sp}*Eff \qquad \text{(eqn. 4-2)}$$

where

A_{sp} is the area of the solar panels in m^2
P_s is the power density in W/m^2
Eff is the Cell efficiency
P is the Energy generated in Watt*hr

The panel area must be manipulated so that the energy accumulated exceeds the energy used with a comfortable safety margin. This has been accomplished and is shown in the power budget (table 4-4).

The solar panel is flexible with a total area of 9.288 m^2. When stowed, the panel fits into the payload bay, rolled into a cylinder against the payload bay's inside wall.

The length of the payload bay is 2.8 meters. The diameter of the payload bay is 1.27 meters, and its circumference is 3.99 meters. The solar panel is therefore 2.795 m wide, and 3.9 meters long. Its thickness is about 0.5 cm.

An initial estimate for the mass and cost of a space qualified solar array with an area of 9.3m^2 is derived from conversations with Shiela Baily at NASA Lewis Research Center, and Ron Diamond at Spectralab Corporation.

Industrial sources quoted the mass as 0.13 grams per square centimeter, with laminates and plate glass cover, but without substrate or insulation. They stated that double this would be a good ball park estimate for the completed structure. This results in a total estimated mass of 12 kg. The mass budget allows for 50 kg, including cabling, stiffeners, and single axis tracking.

The cost of a space qualified solar panel is about $1.4 M/kW. Since space provides 1.44kW/m^2, and the cells are 18.5% efficient, each square meter provides 266 Watts of power in full-illumination. Therefore, each square meter costs $1.4M*0.26 = $364,000. PowerSat requires 9.3 square meters, making the array's cost $3.4 million. The vendor supplies design assistance for custom designed deployment, mounting and interconnection.

As a starting point, 1 mm thick fiberglass panels are specified for the rigidizing structure. The fiberglass will be rigid for 6 cm along its long axis, then have a flexible hinge 0.5 cm wide. This pattern is repeated along the entire structure's 3.9 m length, resulting in 60 rigid sections, each 6 cm wide and 2.975 m long, connected by 59 hinges that are 0.5 cm wide.

This structure is backed with a single Tracor inflatable stiffener. The fiberglass backing will provide stiffness over a small area, and will be flexible only at the 0.5 cm wide "hinges" that occur each 6.5 cm along the entire length of the structure. This supplies enough flexibility to allow the panels to be formed to the outside of the cargo bay when in the stowed configuration.

The glass on the front of the cells prevents the crystalline cells from flexing, with the required flexure occurring at the breaks between the 6 cm cells. The 0.5 cm gap is required to flex enough to bend the structure into a cylinder 1.27 meters in diameter. Since the length of the outside surface of the cylinder is 3.9 meters, there are 59 gaps. Each gap flexes through 360/59 = 6.1°.

As the deployment takes place, the panels are kicked free and allowed to stabilize against the fiberglass' flexible backing. Then the stiffener is inflated, resulting in a rigid, flat panel deployed in space.

The usual method for solar tracking involves a slit with solar energy coming through it, or a shadow board. Optical sensors are placed on the substrate behind so they are both illuminated equally when the sun is directly in front of the array.

If the array orientation is off center, one sensor or the other finds itself in a greater amount of light. This imbalance is fed back to the positioning device on the array, resulting in an error voltage to the positioner motor. The motor drives the array into its proper orientation.

A micro-controller based system will be used, effecting the same function without an analog control system, and many of its common over-damping worries. The serial port on the controller connects to a telemetry system channel, with software for simple ground commands (go to a specific orientation, enter search mode, or track mode as examples). A design for such a tracking system is available from Sandia National Laboratories.

Since this satellite is continuously angled towards the sun in a sun-synchronous orbit, this device is only used for initial positioning.

Thermal considerations for the solar array have been explored with industry. They report that no problem exists regarding the panels' operating temperature.

The best estimate for the stabilized operating temperature in free space and full-sunlight is derived from the space station project documentation. This shows that similar panels with a transparent substrate run at 288° K. It further states that reflective backing increases this temperature by about 15° K. That puts the operating temperature at 303° K.

The solar panels meet military specifications. Designed to operate at temperatures as high as 500° K, they are more than adequate for PowerSat's mission.

Power Routing and Conditioning

The solar panels consist of vertical stacks of cells, each connected to the one below it. Each cell produces about 1 V in full illumination. The 6 cm cell spacing, stacked to 2.8 m, results in 43 cells per stack. Therefore each stack produces a 43 V output. There are a total of 3.9 m/6.5 cm = 60 stacks.

The panels are each divided into 20 groups of 3 stacks, connected in series. This results in a 126 V buss voltage, sufficient to reduce resistive losses in the wire, while controlling the difficulties associated with voltage breakdown. This design also provides adequate possibilities for switched shunt regulation.

PowerSat uses a battery control system that successively switches panels to ground when the batteries are charged.

Each battery cell has a mid-discharge voltage of 1.248 V. PowerSat needs 27 kW*h at 100 V. This makes the battery requirement 80 series-connected cells of 337.5W*h each, or 270 Ah each.

The individual cells have a 1.55 V float voltage, resulting in a 124 V float voltage for each bank. This floating voltage matches the 126 V maximum voltage produced by the solar panels. With this match, pass diodes are used to simply bridge the panel output across the DC bus.

Two banks of 125Ah cells, which are similar to those available commercially, are used, with the exception of the NASA Lewis designed nickel electrode.

Power is supplied to the spacecraft's low-power systems using a redundant system, each consisting of 10 panels, one 80-cell battery bank, and the necessary charging and supply electronics. A malfunction in either system will be transparent. DC to DC converters, and simple monitoring circuitry are commercially available.

Staggered high-voltage powers the magnetrons. A failure in one power system results in alternate magnetrons being denied power. This allows continued operation at half power, but with the radiation pattern effected as little as possible.

The inverter is a micro-controller based device that allows individual magnetron high-voltage control by manipulating the wave form sent to each transformer. The parameters used to derive each wave form can be changed from the ground through a serial link via a telemetry channel.

The high-voltage DC to DC converter supplies each of the 32 magnetrons with 4500 V at 0.8366 A. There is no commercial device that meets this requirement. Since the outcome of a converter development program is uncertain, mass and efficiency numbers are estimates.

Table 4-4 PowerSat Power Budget

Power Generation Capability:

Free space power density	1440 Watts per square meter
Cell efficiency	0.185
Cell size	0.0036 Square meters
Cell voltage:	Vmp= 0.89
	Voc= 1.02
Arrayed as	43 Cells per column
	3 Columns per panel
	20 Panels
Bus voltage	Vmp= 114.81
	Voc= 131.58
Array dimensions	2.795 Meters by 3.9 Meters
For a total area of	9.288 Square meters
For a total power of	2474.323 Watts
In full sunlight for	24 Hours
Providing	59383.75 Watt*hours

Power Storage Capability:

Cell size	125 Amp*hr
Cell dimensions	10 cm diameter
	15 cm length
Cell Voltage	1.55 Volts (float)
	1.1 Volts (EOD)
Number of cells per bank	80
Number of banks	2
Bus voltage =	124 Volts (float)
	88 Volts (EOD)
Stored power per bank	13250 Watt*hr
Total stored power	26500 Watt*hr
	1.59E+06 Watt*min
Battery efficiency	0.85
Depth of discharge	0.72
Transmit power (input)	120500 Watts
Sustained for	8.075352 Minutes

Power Usage:

Main transmitters	120500 Watts	8 Min/day
Telemetry	300 Watts	24 Hr/day
Computer	15 Watts	24 Hr/day
Attitude control (tape)	500 Watts	24 Hr/day
Attitude cont. (gyros etc.)	200 Watts	24 Hr/day
Thermal	500 Watts	12 Hr/day
Total energy used	49621.96 Watt*hr/day	
Total energy collected	59383.75 Watt*hr/day	

Attitude Determination and Control

PowerSat is a three axis gravity gradient stabilized craft. The spacecraft's mission configuration is characterized by two nearly independent structures connected by a gimbal joint. One structure is massive, dense and compact; and the other structure has low-mass and density, but is large. Attitude determination and control follows a master-slave schedule. The spacecraft's main body, the high-mass portion, is the master. The transmission antenna, the low-mass portion, is the slave. PowerSat has no translational control. Due to steering of the phased array transmitter employed by PowerSat, the attitude control system needs only to maintain three degrees pointing on track, and one degree pointing cross-track to the satellites orbit path.

Attitude Determination

The purpose of the attitude determination system is to provide relative orientation information to the attitude control system. PowerSat's attitude determination follows three configuration phases. The first phase is launch through orbit injection. The launch vehicle is responsible for attitude determination during this phase. The spacecraft attitude determination system is in a self-test configuration in order to verify its operation.

Phase two is after orbit insertion. During this phase, the attitude determination system remains in self-test for the first few orbits in order to verify its integrity. If necessary the attitude determination system configures itself around most faults. If the system cannot reconfigure, it notifies the command, control, and communication (C^3) computer. The C^3 computer then attempts an emergency ground station link for further instructions. If the system is undamaged and can configure itself, it begins initial attitude determination using sun sensors. There are ten sun sensors on-board PowerSat: six digital and four analog. The six digital sun sensors are configured in three perpendicular pairs. A pair is located on each of the three sun facing panels of the satellite main body, above where the inflatable antenna attaches.

The other two analog sun sensors are located, one each, on the top and the bottom of the main satellite body. Figure 4-14 illustrates the positions of the digital and analog sun sensors. Data from the ten sun sensors provides adequate information to determine the spacecraft's attitude with respect to the sun. A GPS receiver provides satellite position information, with respect to the Earth, to within 100 m, and a time reference. The total data is sufficient to determine the attitude of the spacecraft, with respect to Earth, with great accuracy. The GPS antennas (shown in figure 4-14) are sampled one at a time. At any time and attitude, there needs to be at least one antenna capable of receiving from at least two GPS satellites to insure GPS operation.

The satellite is then placed in gravity gradient stabilized mode. A scanning horizon sensor, located on the center panel facing the sun, is activated. this

sensor, combined with the data from the six digital sun sensors, allows calculation of PowerSat's attitude to

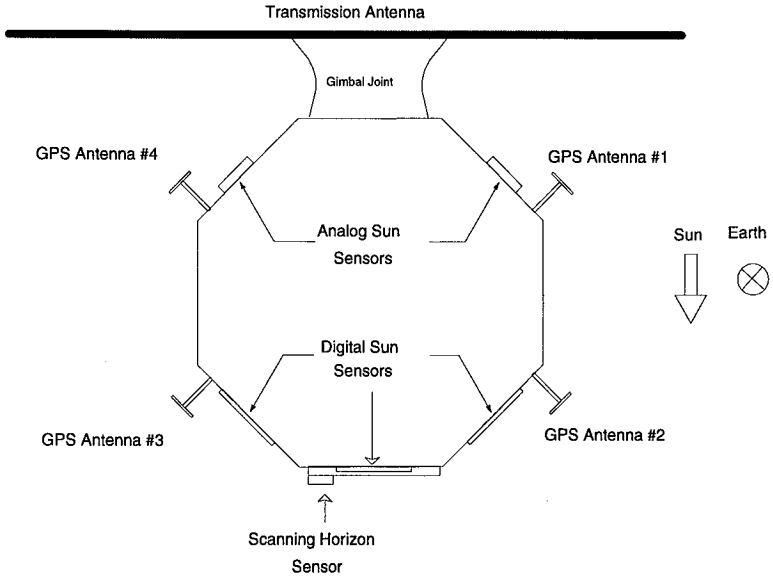

Figure 4-14 Position of Altitude Determination Components

better than one degree of accuracy. The GPS receiver provides redundant attitude information, and a history of its accuracy and reliability is maintained for evaluation as a sole attitude determination system for LEO satellites.

Phase three of PowerSat's mission begins when the satellite has achieved a stable attitude. After the satellite has stabilized in gravity gradient mode for several orbits, the inflatable array is deployed. The attitude of the inflatable antenna is measured with respect to the satellite main body and must therefore be very accurate in order to avoid propagation of errors.

The design suggested by Tracor, consists of lasers, reflectors, and detectors situated on the inflatable antenna and the satellite main body. The control system for the satellite main body is the master system, determining its orientation with respect to the Earth. The inflatable antenna control system is the slave, setting its attitude relative to the satellite main body.

Attitude Control

The attitude control system utilizes the information from the attitude determination system to achieve a stable desired attitude, and maintain it. During phase one, the launch phase, it is the responsibility of the launch vehicle to maintain its own attitude control. All of the control actuators are in a locked and launch-ready state to avoid damage. There are no provisions for testing the control actuators after the satellite has been integrated with the launch vehicle.

During the first part of the phase, the control actuator system will be placed in power on, self-test mode, to verify the integrity of the system. If any failures are noted that will inhibit three-axis stabilization acquisition, the C^3 computer attempts an emergency ground station link to obtain further instructions. If the control system is undamaged, it waits for the attitude determination system to finish its tests and provide attitude data. Centrally located in the satellite main body are three zero bias momentum wheels: one high-inertia wheel with its rotational axis parallel to the satellites major axis, and two low-inertia wheels, all orthogonal to each other. There is no redundancy in this system, and it represents a single point failure mode for the control system. High Mean Time Between Failure (MTBF) components are required. The three momentum wheels are used to obtain an initial three-axis stabilized orientation. On its earth-side, PowerSat uses a 10 m telescopic boom with a 20 kg mass at the end to allow it to obtain an attitude. The effect of the mass and the boom is to increase the length of the major axis of the craft sufficiently to allow for gravity gradient stabilization. The two smaller momentum wheels are used solely for initial attitude acquisition, and then shut off. Six libration dampers are used to damp the librations sufficiently. There are three dampers at the top of the main body, and three at three at the bottom arranged as shown in Figure 4-15.

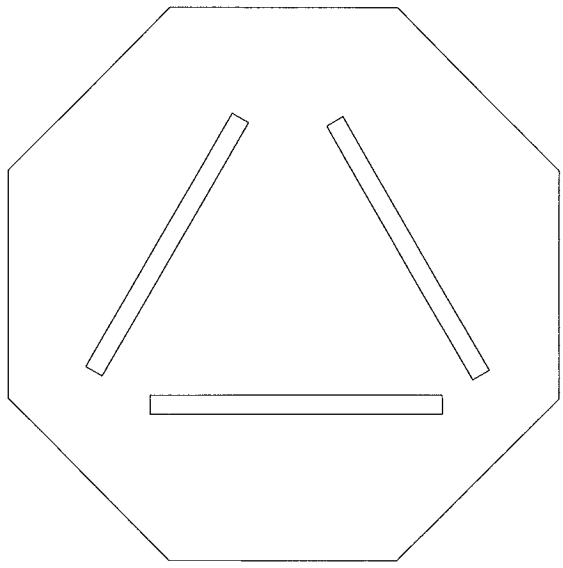

Figure 4-15 Liberation Damper Configuration

At this point the attitude determination system switches on the scanning horizon sensor. The scanning horizon sensor is specified with a very high momentum bias, and will act as a reaction-type passive control in the two rotational axis not controlled by the gravity gradient stabilizer. The spacecraft

then is allowed a substantial settling time before it enters phase three.

In phase three, the inflatable antenna is deployed. At each of the inflatable antenna's four corners is a small three-axes, zero-bias momentum wheel module. The momentum wheels are specified with magnetic dipoles, located on their inertial rings to allow momentum dumping into the Earth's magnetic field. The units are specified by Tracor.

Heat-tape is wound around the antenna's major inflatable supports. The heat tape provides the shape of the inflatable antenna thermal expansion control. The four momentum wheel units provide moments on the antenna through a gimbal joint attachment to the satellite main body.

The main body of the spacecraft provides only three to five degrees of accuracy in its attitude, but can measure its attitude to within half a degree. The attitude determination and control system for the antenna, corrects for the inaccuracy of the satellite main body with its very precise laser sensors. Because the antenna operates in closed loop with the ground site, the antenna control system can be calibrated for greater accuracy if desired. The momentum wheels in the satellite main body do not have a momentum dumping mechanism because the secular forces on the satellite will not saturate them within the satellites nominal three-year mission. Figures 4-16a and 4-16b are block diagrams of the attitude determination and control system for the Satellite main body.

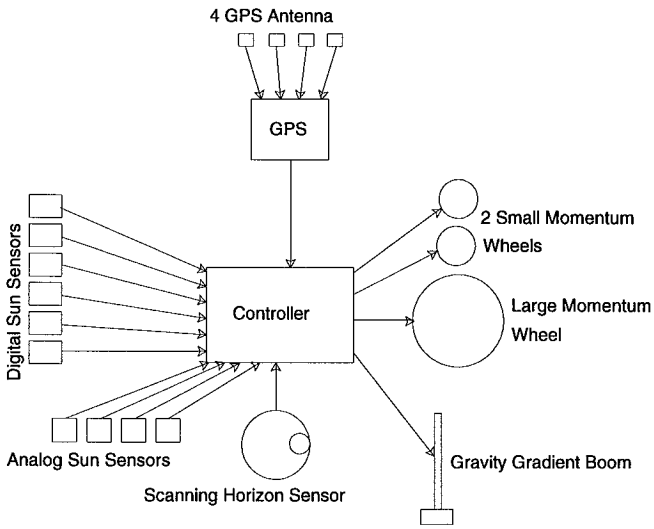

Figure 4-16a Atitude Determination and Control System

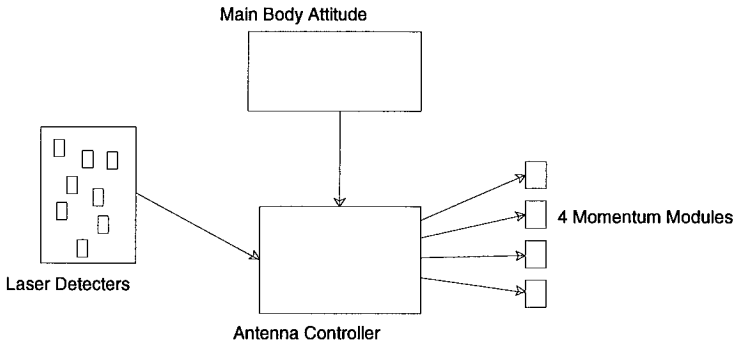

Figure 4-16b Attitude Determination and Control System

Attitude Pointing

The attitude pointing system's primary accuracy concern is to stabilize the phased array antenna with the ground station. Using a phased lock loop arrangement, the phased array's beam steering is automatic. For the PowerSat project, the ground station transmits a beacon at twice the transmit frequency (4.90 GHz) of the power beam transmission (2.45 GHz). This beacon is received by the power beam transmission array and is used to control the power beam transmission phase shifters. Figure 4-17 demonstrates how this is accomplished.

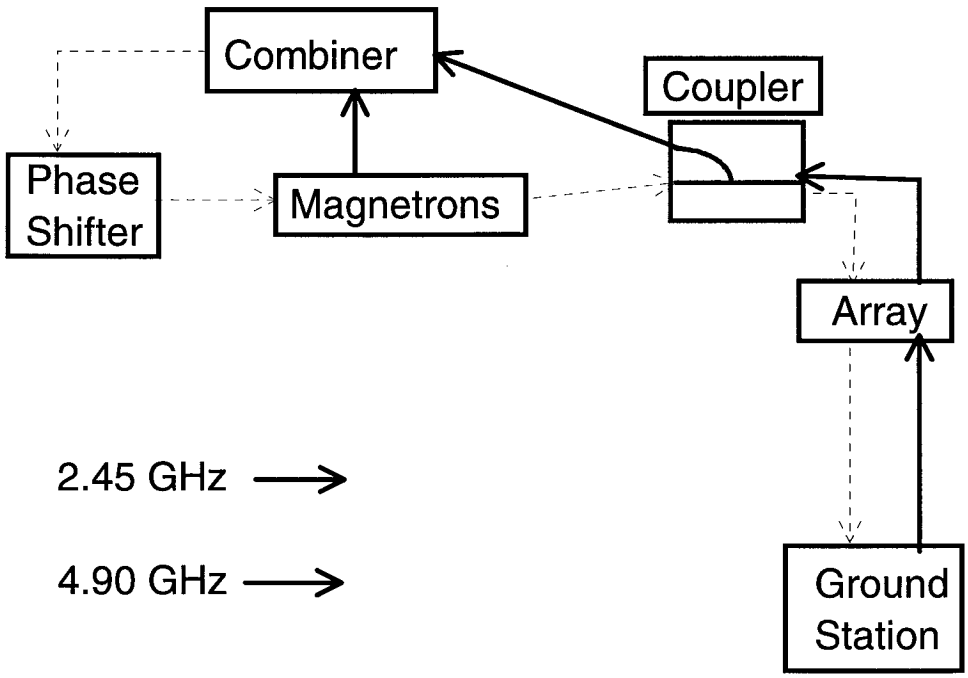

Figure 4-17 Signal Flow Diagram for Phase Steering of Antenna

Steerability of Antenna Array

The capability of the antenna to track a ground target can be analyzed in two dimensions: in-track (along the major axis of the array), and cross-track (along the minor axis of the array). The maximum array steering angles are based on the following factors:

a) The point at which the array pattern becomes "endfired." This is the point where the beam main lobe begins to intersect the array plane.
b) The array space factor that determines the array's gain and radiation patterns.
c) The grating lobes effects and quantization levels.

These effects tend to influence the array's overall performance and can be considered as losses in the array's efficiency. For example, in a direct broadside array, where the individual elements are all in phase, the array's gain can be represented by equation 4-3.

$$Gain = \frac{4 \cdot \pi \cdot L \cdot W}{\lambda^2} \qquad \text{(eqn. 4-3)}$$

Where

L is the array's length = 32 meters
W is the array's width = 18 meters
λ is the transmitted signal wavelength = 0.122 meters

Grating Lobes

The next consideration is to determine at what steering angle grating lobes appear. Grating lobes are a function of the steering angle and the ratio of the element separation to the wavelength. This function is:

$$\frac{d}{\lambda} = \frac{1}{1 + \sin(\theta_s)} \qquad \text{(eqn. 4-4)}$$

Where

d is the separation distance between elements
λ is the signal's primary wavelength
θ_s is the steering angle of main beam from broadside

For the 0.618 wavelength spacing, which is the maximum achievable for the TE_{11} mode in a circular waveguide, a maximum steering angle of +/- 38° is obtained from broadside without grating lobes. Higher steering angles are achievable if the array's gain reduction is accepted. This gain loss actually appears as energy in the grating sidelobe.

This is possible since the energy in the grating lobe falls under a sinusoid envelope. The total energy in the system remains constant, so the main beam gain falls off only slightly as the grating lobe increases until they equalize. At this point, the grating lobe can actually be considered the array's main beam. Figure 4-18 shows how the grating lobe increases as the main lobe decreases.

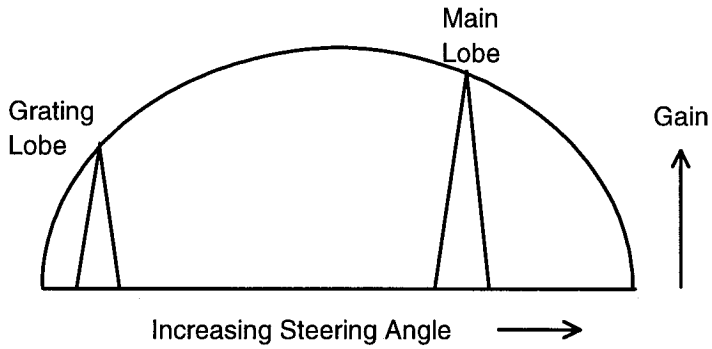

Figure 4-18 Comparison of Grating Lobe Gain to Main Lobe Gain

This analysis shows that the present satellite array will not be able to beam power to the Earth station during its entire above horizon duration. Since the array's steering angle, the Earth central angle, and the elevation angle plus 90°, form a triangle, we can estimate the maximum steering amount that the satellite will need to accurately acquire the receiving site during a full pass. Figures 4-19a and 4-19b give these values and show the triangular relationship.

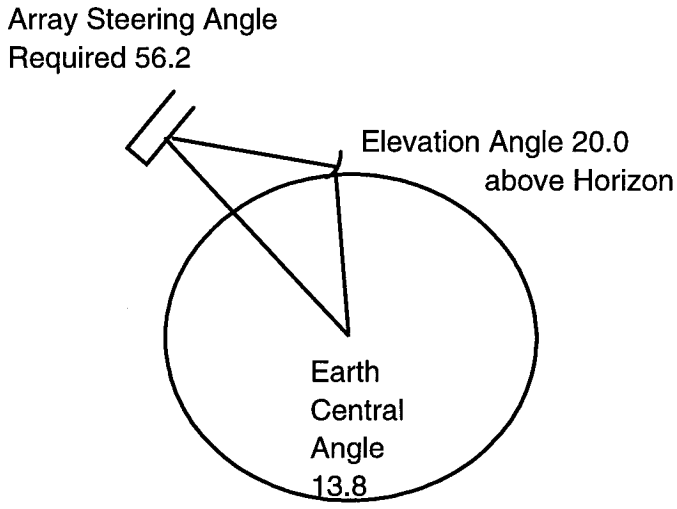

Figure 4-19a Triangular Relation between Earth central angle, steering angle, and elevation angle.

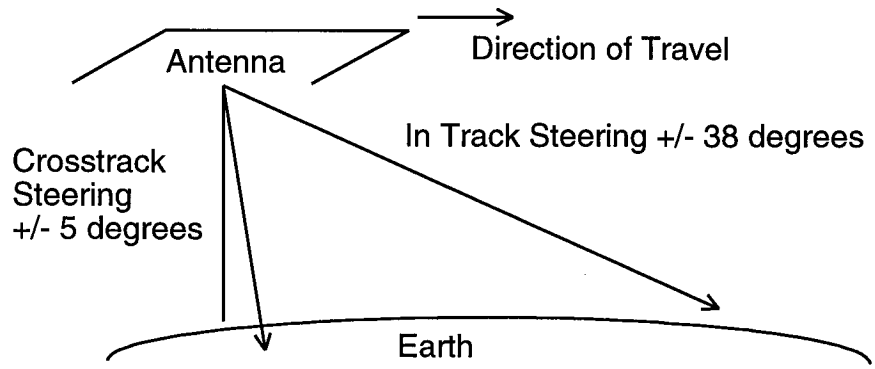

Figure 4-19b Triangular Relation between Earth central angle, steering angle, and elevation angle.

Since the current array design cannot accommodate the 56.2° steering angle, the reduction in beaming time (to about 6.2 minutes) must be accepted, or the antenna must be redesigned for increased steerability. The final antenna design will be a funded project design team's concern.

Feasibility

The current array design does meet requirements. It does electronically acquire the target receiver site for more than six minutes per pass. Using a ground beacon phase lock loop, it can accurately steer the transmitted microwave power beam onto the receiving array. The feedback provided by the phase lock also overcomes small transmitted beam deformations.

Based on these assumptions, any error in the attitudinal positioning of less than 3° can easily be accounted for by the array steering itself. A greater than 3° error causes problems, not with the power beam steering, but with the appearance of the first grating lobe, and a lower than expected gain and power transmission. This skews the results of any efficiency tests.

Safety

The appearance of grating lobes does not offer any safety problems because their appearance is at 90° from broadside, and will radiate harmlessly into space. The greatest concern is unintentional interference with communication satellites inside the grating lobe. Communication satellites will experience a PowerSat EIRP of 89.6 dBw signal. To avoid this possibility, grating lobes must be avoided, and a sufficient margin of error built into the pass time to ensure that the array beaming angle is below 38° at the beginning of any power transmissions.

Conclusion

Under the given limitations, PowerSat is fully capable of maintaining adequate positioning to ensure that effective space-to-Earth power beaming experiment determination may be conducted without causing any interference with existing communications facilities. Please note however that as part of the phased array's final design process, certain questions must be answered to ensure precise microwave power beaming efficiency level measurements to ensure noninterference.

Future Considerations

The following criteria/questions must be answered during the final array design process:

a) Determine which communication satellites may be impacted by the appearance of grating lobes and worst case effects.
b) Verify that the design meets certain minimum grating lobes criteria. Specifically, that the array's theoretical and actual steering angle limit have a sufficient built in safety margin.
c) Verify the actual array gain figures since some present efficiencies are based on assumption. Actual array gain figures will effect the beam width, and determine the safety area required on the ground.

Satisfying all these requirements will successfully be accomplished by a research institute in conjunction with the contractual source for the array, and will be accomplished during the initial design process.

COMPUTER AND INSTRUMENTATION

Computer System

The computer subsystem will serve as PowerSat's central controller. All the attitude determination information will be processed by the computer subsystem, and data will then be sent out to the control actuators. The computer subsystem will also provide a collection point for all that will be transmitted to the ground via TDRSS. The computer subsystem provides a central hub that is essential to the PowerSat's operation.

A Fairchild Space FS386 is PowerSat's primary computer system. The FS386 provides a stable, configurable and expandable system from which the command and control can be exercised. The basic FS386 system consists of an enclosed backplane bus system, to which various cards can be attached. The available cards are as follows:

Processor Card

This card holds the CPU for the system. It is possible to use multiple cards for redundancy. The system uses an industry standard Intel 80386 running at 32 MHz as its processor. Additional components include an 80387 coprocessor, 512 Kb SRAM for application code, 384 Kb EEPROM for boot loading and program storage, a RS-232 port for testing and external interface, and fault-tolerant features.

Memory Card

The memory card provides the main memory for program execution. The card provides 6.6 megabytes of SRAM. The memory is able to correct single bit errors and detect double bit errors in the 7-bit memory.

Telemetry and Command (T&C) Card
This card provides the interface to the external instrumentation and control devices. The T&C card provides one differential analog command channel, 16 serial digital command channels, 64 telemetry channels and 1-28 V pulse with programmable duration.

Transponder Card
The transponder card provides uplink and downlink interfaces with built in redundancy. The uplink features Dual redundant transponders, TDRSS compatibility and rates from 100 BPS to 200 KBPS. The downlink provides TDRSS compatibility and a dual channel 6 MBPS aggregate data rate.

The Power Converter Card
This card provides power to the FS386 system.

PowerSat's configuration needs require dual processors cards, a single T&C card, and a single power converter card. The transponder card is not necessary. A computer subsystem block diagram is shown in figure 4-20.

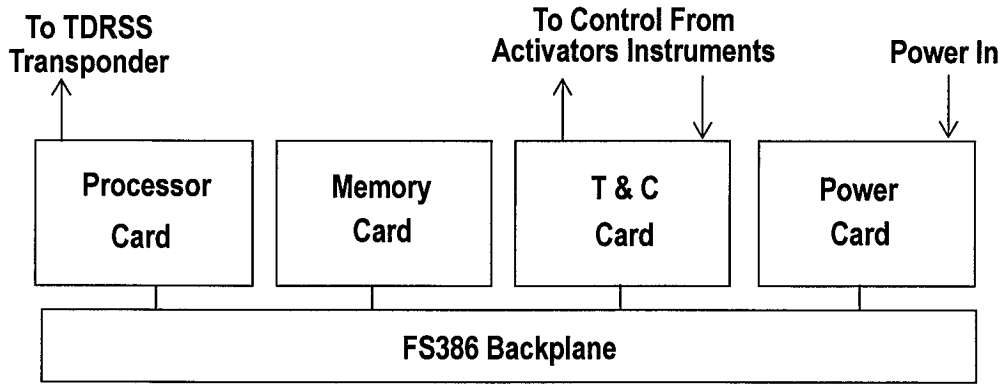

Figure 4-20 FS386 Block Diagram

COMMUNICATIONS SUBSYSTEM

System Overview

The communication system is responsible for receiving and transmitting satellite link data. Primarily the satellite conditions is transmitted, and most of the attitude control is accomplished with on-board satellite processors. Access to the satellite's control system is, very importantly, for fail-safe purposes. Therefore, the link does not have a very demanding bit rate. It is convenient to have the ground control at the same site as the power receiver for readily available telemetry information.

Prior to power beaming, a beaming code is sent up to PowerSat, indicating that the ground station is ready to receive the 2.45 GHz signal. A beaming

code also assures no inadvertent beaming to stray 4.9 GHz beacons. This beaming code prepares PowerSat to receive the beacon and enable power beaming.

System Constraints

The link is, of course, limited to federal laws regarding frequency selection. Frequency allocation will need to be obtained. Some delay is acceptable for information transfer for most instantaneous commands, with the exception of the beaconing switch on-board PowerSat.

System Configuration

For several reasons, TDRSS has been selected for the telemetry responsibility. A TDRSS Earth station is conveniently located at White Sands Test Facility. Also, for satellite configuration reasons, locating the telemetry antenna on the top of the satellite avoids conflicts with the phased array and deployment. In addition, the TDRSS transponder gives almost 80% coverage allowing for array preparation, whereas a direct link has only minutes to communicate. The free space losses in trying to beam from 843 km to geosynchronous orbit is greater than beaming down to earth, however, the advantage is the ability to set up a ground site at various locations, and not be limited by the telemetry link.

NASA's Tracking and Data Relay Satellite System employs two geosynchronous satellites at 45°W and 170°W. At the present altitude of 843 km, PowerSat will not receive full coverage, but as mentioned before, will maintain contact for approximately 80% of the time. The exception is approximately 60°E to 90°E, which is somewhere in the vicinity of India. Future expandability to other sites will be fairly simple with this centrally located communication ground control station. Figure 4-21 is a block diagram of the communication system.

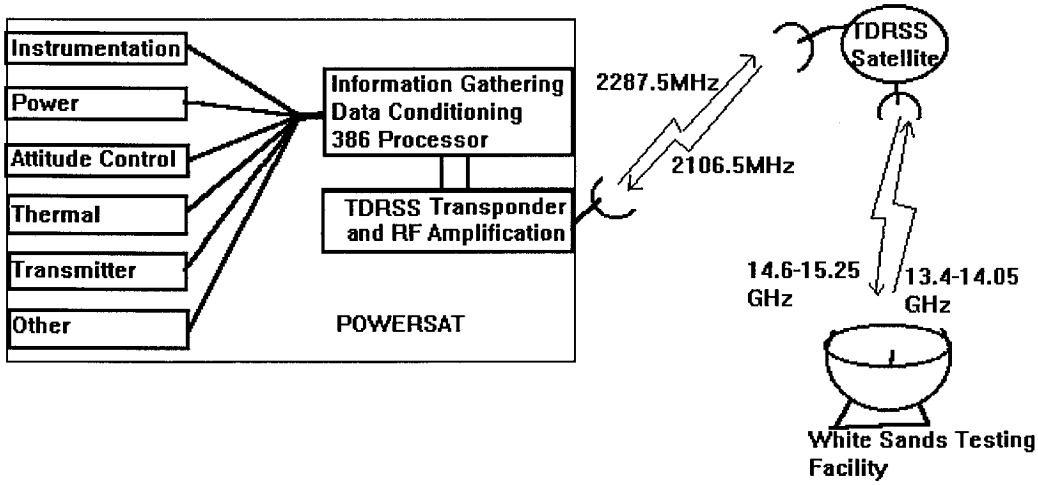

Figure 4-21 Communication Block Diagram

Link Characteristics

PowerSat uses a multiple access link that will provide an S-band 2287.5 MHz uplink, and a 2106.4 MHz downlink to the satellite. By using the multiple access configuration, communication is limited to a data rate of 1000 bits/sec, which is more than sufficient for supplying satellite conditions to earth station observers. Table 4-6 provides some telemetry system characteristics.

Table 4-6 Communication Specifications

Freq (command link) (MHz)	2106.41	Freq (telemetry link) (MHz)	2287.5
Power transmitted (Watts)	100	Power transmitted (W)	5
Gain Trans Antenna (dB)	19	Gain Trans Antenna (dB)	14.55
Line Loss (dB)	1	EIRP	21.53970004
EIRP (dB)	38	TDRSS ant gain (dB)	19
PowerSat ant. gain (dB)	13.546		
Free Space Loss (dB)	190	No	6.9E-18
Dist.(Psat-TDRSS)(km)	34949	Eb (command link)	1.79721E-14
Ts (assumed) (K)	500	Eb (telemetry link)	1.13232E-15
R (bps)	1000		
Pr (at PowerSat) (dB)	111.464		
Pr (at TDRSS) (dB)	122.470		

Beacon

A beacon will be set at the power ground station location providing the satellite power transmitter with a coherent 4.9 GHz (twice the power beaming frequency) signal. In addition to providing a coherent signal for phase "steering," the beacon will serve as a fail-safe for unintentional power beaming, because power will be transmitted only when this signal is "seen" by PowerSat, and prior permission has been given via the telemetry system.

THERMAL SUBSYSTEM

Thermal Considerations

The function of the thermal control system in a spacecraft is to maintain the temperatures in some sections of the spacecraft within certain temperature ranges, ensuring the proper operation of the spacecraft subsystems. In general, several subsystems in a spacecraft need to consider the ambient temperature and the thermal dissipation. The subsystems in the PowerSat project include the microwave generating devices, the electronic units for telemetry, instrumentation, altitude control, and electrical power supply. In addition, the thermal properties of the spacecraft surface are also design objectives, which governs the global thermal exchanges between the spacecraft and the space environment.

Temperature ranges for PowerSat's components are listed in table 4-7.

Table 4-7 Typical Temperature Ranges for Some Major Components of Spacecraft

Components	Temperature Range° C
Electronics	0 to 40
Batteries	-10 to 20
Solar Arrays	-100 to 100
Power Electronics	0 to 80
Transformer	-50 to 150

There are three thermal exchange principles: conduction, convection, and radiation. Due to the absence of the air and other thermal mediums for conducting and convecting in space, radiation is the only major principle that governs spacecraft thermal behaviors. The radiative thermal exchange is characterized by the equation:

$$q = \varepsilon\sigma T^4 \qquad \text{(eqn. 4-5)}$$

where

q is radiated thermal energy in W/m^2
ε is the emissivity, a dimensionless number between 0 and 1
σ is the Stefan-Boltzmann constant
T is the radiating surface temperature in Kelvin

The other thermal exchange principles may be used in rare cases, but it is usually just for the local thermal exchange only.

Spacecraft Waste Heat Sources

The thermal waste in a spacecraft comes from two aspects, radiation from the Sun and the Earth, and the thermal dissipation from the electronics in the cabin.

The average radiation flux is 1358 W/m^2 from solar in a narrow spectrum, and 237 W/m^2 reflected from Earth in the infrared spectrum.

Within the spacecraft cabin, the microwave power generating device is the major waste heat source. Using the currently selected magnetron, with up to 85 percent efficiency, this subsystem needs to dissipate up to 12.4 kW thermal loss, based on the beaming power of 70 kW. Another waste heat source is the magnetrons' anode high-voltage power converter. In this unit, waste heat comes from several kinds of components, such as batteries, transformers, solid relays and power switch devices. With 85 percent of specified battery efficiency, the waste heat from the battery banks is 15 kW during full power

discharging time. From the transformers, the waste heat is up to 4.6 kW. These two subsystems produce much more waste heat then the rest of the subsystems combined. The remaining subsystems produce less than 900 W waste heat.

Thermal Control System Overview

Based on the current geometrical configuration, as shown in figure 4-21, and the selected orbit, the thermal control system has the following features:

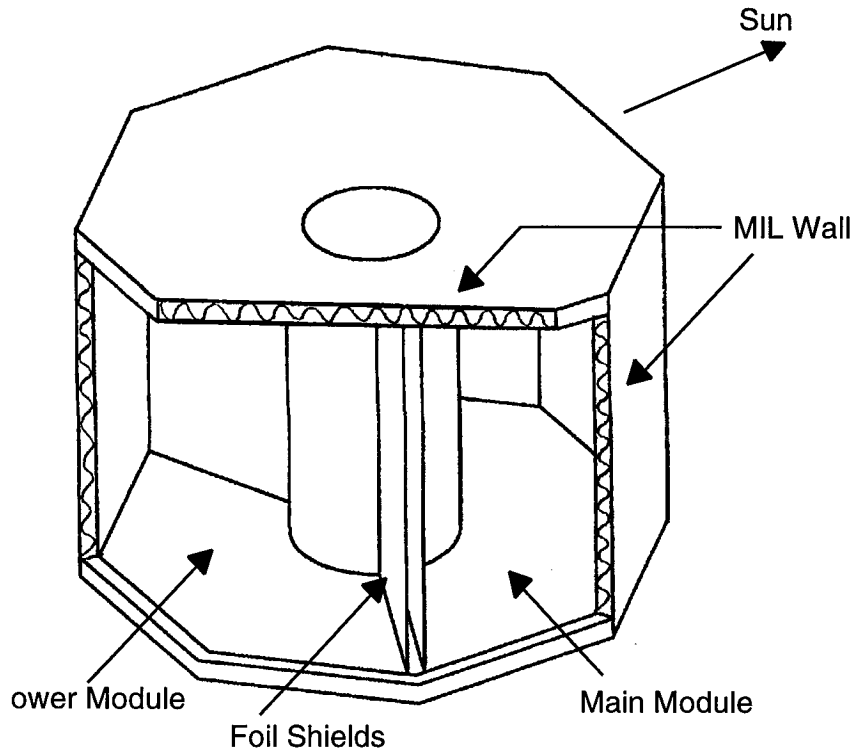

Figure 4-21 Diagram of Radiation Shielding

As the microwave generator and a major waste heat source, the magnetron assemblies are installed beside the power beaming antenna to obtain higher efficiencies on both the thermal dissipation and microwave delivery.

The spacecraft cabin, with a polygonal plane view, is implemented with complex insulation board (MIL), providing a protection shell for all of the subsystems. Due to the sun-synchronous orbit, each side of the cabin has almost constant, but different solar energy flux incident densities. For this reason, different thermal control coatings may be applied to the different surfaces accordingly. For example, finishing the surface that is constantly facing the sun with white enamel that has a ε/α value of 0.35, gives a 308.3 K balanced temperature.

The power convertor unit, another major thermal source, is located against the cabin's shadowed wall. The rest of the equipment is located on or against the wall directly facing the Sun. In this arrangement, waste heat created by

the transformers, batteries and other power devices can dissipate directly to black space. Since the power convertor only works during the beaming time, about 7 minutes per pass, the insulation between the power convertor unit and the others should not be difficult to attain.

With properly designed thermal insulation walls and surface coatings, the system can function without any active cooling equipment. However, to ensure temperatures do not drop below adequate ranges for the subsystems within the cabin, electrical heaters keep the temperature stable. These units may need up to 500 W electrical power in a discontinuous working pattern.

As shown in figure 4-22, a PDI controller is used to control the heaters. This will be accomplished with a microcontroller, through the I/O port where the temperature information is collected and sent to the main computer in the cabin. Meanwhile, the control command from the main computer (if any) can also be received through the I/O port.

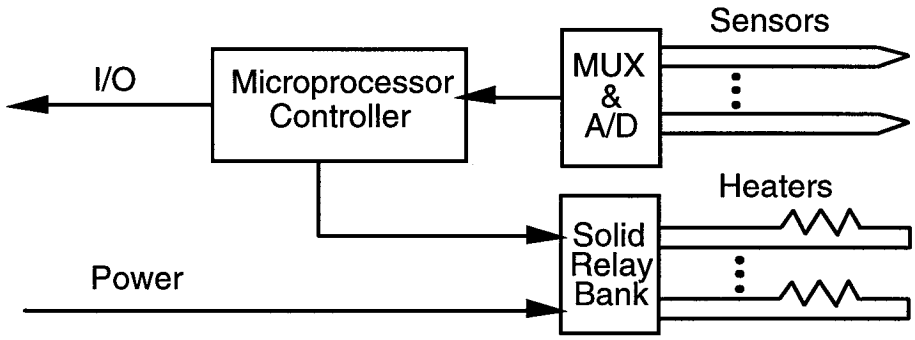

Figure 4-22 Thermal Control Processor

Calculation and Analysis

Evaluating the thermal control system involves solar energy calculation, waste heat estimation and thermal analysis.

The first item, in principle, is a set of geometrical calculations through which the solar energy on the surface of the spacecraft cabin is obtained as the function of surface orientation, by measuring the angle between the surface normal and the Sun incident direction. In a sun-synchronous orbit, all these angles are constant.

The second item, the waste heat within the cabin, mainly relies on final designs of the other units. This includes their dissipated power, their geometry features and locations in the cabin.

Once these calculations and designs are done, the thermal analysis can be performed based on their results.

In general, by discreting the surface of the whole system into n elements, each of which has an area δA, and δV_i, a share of the volume that is sur-

rounded by a group of surfaces, and using the constitutive equation 4-5, the equation in discrete form for the whole system can be written as:

$$p_i c_i \delta V_i \frac{\partial T_i}{\partial t} = -\sum_{j=1}^{n} \varepsilon_i \sigma F_{ij} \delta A_i \left(T_i^4 - T_j^4 \right) + q_i \qquad \text{(eqn. 4-6)}$$

$$(i=1, 2, ..., n)$$

where

T_i and T_j are the temperatures of element i and j, respectively

ρ_i is the density of the element i

c_i is the thermal capacity of the element i

δV_i is the volume share of the element i

F_{ij} is the diffuse view factor from element i to j, which will be discussed later

δA_i is the area of the element i

q_i is the thermal source in element i

ε_i is the emissivity of the element i

σ is as mentioned before

This equation is for the non-steady state, or time dependent thermal process, that corresponds to the transition process during the beaming time. For the steady state case, the left side of equation 4-6 is equal to zero and q_i is a constant.

To use equation 4-6, it is necessary to estimate and calculate the ε_i's and F_{ij}'s, a emissivities group, and diffuse view factors, respectively.

The diffuse view factor, also known as the angle factor, is a dimensionless number that is defined as the radiated energy fraction leaving surface A, that is intercepted by surface B. Considering the radiative thermal exchange between two finite areas A_i and A_j, as shown in figure 4-23, the total energy leaving A_i toward A_j is

$$Q_{ji} = \int_{A_i} \int_{A_j} I(r_i) \frac{\cos\theta_i \cos\theta_j}{\pi S^2} dA_j dA_i \qquad \text{(eqn. 4-7)}$$

where

$I(\boldsymbol{r}_i)$ is the energy intensity leaving the surface A_i

S is the distance from A_i to A_j

θ_i and θ_j are the angles between the line connecting the A_i and A_j and the surface normals $\boldsymbol{n}_i$ and $\boldsymbol{n}_j$, respectively.

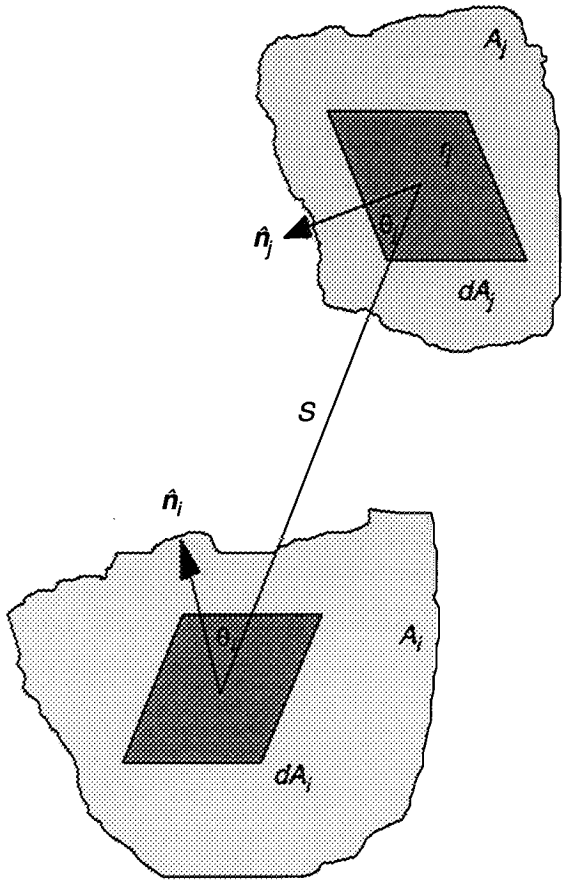

Figure 4-23 Radiative Thermal Exchange Between Two Finite Surfaces

Assuming that the intensity leaving A_i does not vary across the surface, which is true for diffuse-gray surfaces, the angle factor can be written as:

$$F_{ji} = \frac{1}{A_i}\int_{A_i}\int_{A_j}\frac{\cos\theta_i \cos\theta_j}{S^2} dA_i dA_j \qquad \text{(eqn. 4-8)}$$

According to this general formula, the angle factor for any surface pairs can be calculated. Figure 4-23, shows two groups of surfaces forming two modules. For each module, there are 8 and 10 surfaces, respectively, including the top and bottom surfaces. Considering symmetry, the identical angle factors may reduce to 10 and 18 for each module, respectively. For actual thermal analysis, all of the subsystem unit component surfaces installed in the cabin have to be included. For some angle factors, some available formulas are used instead of doing the integral. To perform the thermal analysis, these values are required.

Once these values have been calculated, in addition to the initial conditions (assigned internal and estimated external temperatures), the thermal analysis can be performed by using equation 4-6.

However, as noted, equation 4-6 is non-linear. It is better to linearize it, making the solving process easier. This is done by rewriting it in the conduction form as:

$$p_i c_i \delta V_i \frac{\partial T_i}{\partial t} = -\sum_{j=1}^{n} \varepsilon_i \sigma F_{ij} \delta A_i \left(T_i^2 + T_j^2 \right) (T_i + T_j)\ (T_i - T_j) + q_i$$

$$= \sum_{j=1}^{n} h_{ij} (T_i - T_j) + q_i \qquad \text{(equ. 4-9)}$$

$$(i=1, 2, ..., n)$$

where

h_{ij} is obviously a function of ε_i, F_{ij}, δA_i and temperatures T_i and T_j

Equation 4-9 can be further discreted in time domain as:

$$T_i^k - T_i^{k-1} = -\sum_{j=1}^{n} \frac{\Delta t}{p_i c_i \delta V_i} h_{ij} \left(T_i^k - T_j^k \right) + \frac{\Delta t}{p_i c_i \delta V_i} q_i^k$$

$$= \sum_{j=1}^{n} \overline{h_{ij}} \left(T_j^k - T_i^k \right) + Q_i^k \qquad \text{(eqn. 4-10)}$$

$$(i=1, 2, ..., n;\ k=1, 2, ..., m)$$

where

Δt is the length of the time step

k is the sequence number of the time step

$$\overline{h_{ij}} = \sum_{j=1}^{n} \frac{\Delta t}{p_i c_i \delta V_i} h_{ij} \qquad \text{(eqn. 4-11)}$$

$$Q_i^k = \frac{\Delta t}{p_i c_i \delta V_i} q_i^k$$

Equation 4-10, can be rewritten in the following form:

$$\left(1 + \sum_{j=1}^{n} \overline{h}_{ij}\right) T_i^k - \sum_{j=1}^{n} \overline{h}_{ij} T_j^k = Q_i^k + T_i^{k-1} \qquad \text{(eqn. 4-12)}$$

$$(i=1,2, ..., n; k=1, 2, ... , m)$$

This is a set of T^k linear equations, that can be solved in any method. However, considering its non-linear coefficients, the iterative process is required in each time step.

$$\left(1 + \sum_{j=1}^{n} \overline{h}_{ij}\right) T_i^k - \sum_{j=1}^{n} \overline{h}_{ij} T_i^k + Q_i^k + T_i^{k-1} \qquad \text{(eqn 4-13)}$$

$$(i=1, 2, ..., n; k=1, 2, ..., m)$$

This is a set of linear equations of T^k that can be solved in any method. However, considering its non-linear coefficients, the iterative process is required in each time step. The block diagram of the computation process is shown in figure 4-24.

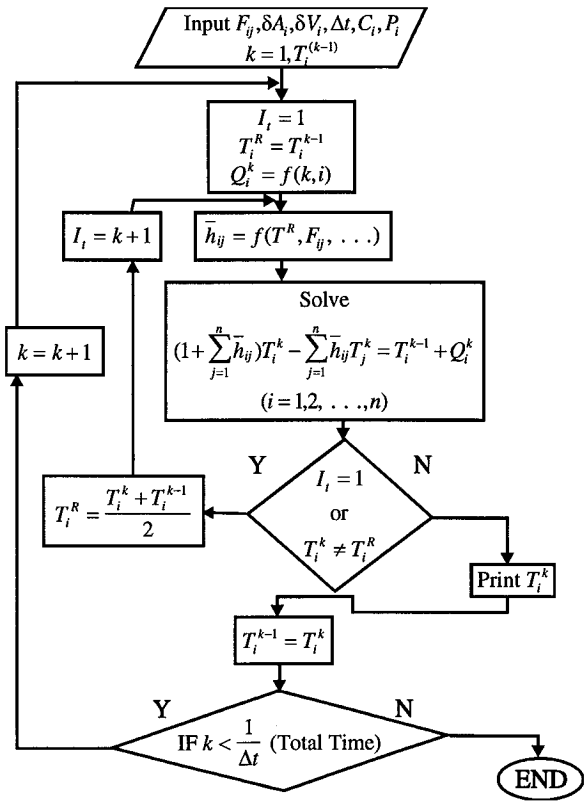

Figure 4-24 Block diagram of computation process.

For the steady state case, equation 4-12 becomes:

$$\sum_{j=1}^{n} h_{ij}T_i - \sum_{j=1}^{n} h_{ij}T_j = q_i \qquad \text{(eqn 4-14)}$$

$$(i=1, 2, ..., n)$$

where

h_{ij} T_i, T_j and q_i are as defined in equation 4-9.

The solution T_i is the temperature at each surface.

SECTION 5 THE MISSION

MISSION IMPLEMENTATION

In order to consider the implementation of this mission, two requirements need to be studied. The first is the cost of the mission. The second is the schedule of the mission.

COST ESTIMATIONS

The initial cost budget was set at $500 million. This amount was chosen based on recent trends for national space projects and the desire to make this proof of concept a national effort. Though this was the initial design constraint the design team placed an emphasis on trying to significantly reduce the budget in order to make the project's scientific merit more appealing. The current status of the design is found in Table 5-1.

Table 5-1 Cost Estimate

Subsystem	**Cost in millions**
Ground Station	.5
Power Transmission	.1
Inflatable Phased Array Antenna **Estimate based on conversations with Tracor, Inc.**	**15**
Solar Arrays 3.4	**5**
Batteries	**2.7**
DC Converters	.1
Attitude Control	3.0
Communications	.2
Structure	1.8
Launch Vehicle: Taurus	**30**
Operational cost for 3 yr. lifetime	15
Total	**73.4**

PROJECT SCHEDULE

The project schedule for implementation of this preliminary design includes rigorous study of design aspects correcting any possible oversights or errors. After this study, the design is to be implemented in phases. These phases include the design and testing of the individual subsystems, redesigns based on any limiting factors found in testing, manufacturing of the systems, and launch and sequence of the mission.

Development Phase

Although one goal of the project is to use current technology as much as possible, the design leads to areas where the technology has not made the subtle changes required for PowerSat application demands. A large inflatable transmitting array, low-weight fast-discharge batteries, and a high efficiency DC to DC converter all need more development. Please note that this development phase is an easy logical step for all industry concerned.

Testing Phase

Every subsystem needs to go through a testing phase to ensure that the characteristic of each system conform to their design models. One of the major areas of testing is the deployment of a large inflatable array in a zero-gravity environment.

Design Finalization

Any necessary design changes will be made, and corresponding changes to dependent subsystems will also be taken into consideration.

Coordination Phase

Each subsystem has a lead time for manufacture. Each should be considered and processed according to a project schedule for finalization and desired launch dates. Some subsystem may have critical components which should be manufactured and acquired first.

Final Testing Phase

Tests should be run to ensure good working interaction between all the subsystems.

Launch

Launch scheduling is a function of the launch vehicle, desired launch date, launch window, and weather at the site.

Sequence of Mission

Most of the PowerSat design is a hardware and software implementation, but some consideration is given to the sequence of the mission. The launch vehicle places the satellite within 3× of desired orbit. The solar panels deploy and acquire the sun. The attitude of the spacecraft is established using on-board attitude and control system for as many orbits as necessary. Once the spacecraft is stable, the subsystems test and report using the available communication link. When the subsystems' operation are verified, the craft takes approximately 10 minutes to deploy the phased array. The phased array control and stability is established using its attitude determination and

control algorithm for as many orbits as necessary. Communication is necessary after the phased array antenna successfully deploys and stabilizes. Microwave experiments can begin at this point.

SECTION 6 CONCLUSION

MISSION SUCCESS CRITERIA

The design team has selected success criteria for the mission. The first criterium is the collection of enough useful data to further solar power satellite development. This information will be gathered over a time span that will allow noting trends during seasonal and yearly variations. The second criterium is receiving the predicted amount of power, proving the solar power satellite idea. The third criterium is testing new technologies, including inflatable support designs for large structures in space.

PROPOSED NEXT STEP

PowerSat's design focuses needs for future design projects. One area which will need further testing is the DC power conversion. Currently there is no space tested commercial DC converter to provide power to the magnetrons. A complete design needs to be tested for the DC power conversion. Development and testing should also proceed in the area of deployable antenna technology. The significant benefits of using inflatable technology at this point needs to be followed by testing of the system.

The operation of PowerSat could include collaboration with other universities or countries interested in studying the effects of high-power transmission through the atmosphere. A series of tests could be launched on sounding rockets to provide valuable information on power beaming through the troposphere and ionosphere. These are tests necessary to pursue the global model. Collaboration could enhance the study of high-power electronics in space, and the effective breakdown in high-vacuum.

PowerSat's design team realizes that further subsystem integration and refinements are necessary for the project's completion, but are excited about the possibilities.

SECTION 6 CONCLUSION

NOTES

SECTION ONE

1) Space Solar Power Program, Final Report, International Space University, Kitakyushu Japan, August 1992.

2) US Department of Energy, Satellite Power System (SPS) Concept Development and Evaluation Program Plan: July 1977-August 1980, DOE/.ET-0034. US government Printing Office, No. 061-000-00031-3, Washington, DC, 1978.

3) Space Solar Power Program, Final Report, International Space University, Kitakyushu Japan, August 1992.

4) M. Nagatomo, N. Kaya, and H. Matsumoto, "Engineering aspect of the Microwave Ionosphere Nonlinear Interaction eXperiment (MINIX) with a Sounding Rocket", Acta Astronautica, No. 13, p. 23-29, 1994.

5) NASA, Solar Power Satellite System Definition Study Part I and Part II, Vol II., Technical Summary, D180-22876-2, December 1977.

SECTION TWO

1) William C. Brown, "Experimental Radiation Cooled Magnetrons for Space" Final Draft of Paper Presented at SPS '91, April 10, 1991.

2) William C. Brown, "The SPS Transmitter Designed around the Magnetron Directional Amplifier" Space Power, Vol 7, No 1, pp. 37-49, 1988.

3) "Conference on Free Space Power Transmission," NASA Lewis Research Center, Cleveland, Ohio, March 29-30, 1988.

4) Louis J. Ippolito, "Radio Propagation for Space Communications Systems" Proceedings of the IEEE, Vol 69, No 6, pp. 697-727, June 1981.

5) William C. Brown, "Beamed Microwave power Transmission and its Application to Space" IEEE Transactions on Microwave Theory and Techniques, Vol 40, No 6, pp. 1239-1250, June 1992.

6) W. E. Scharman, "Breakdown Limitations on the Transmission of Microwave Power Through the Atmosphere" IEEE Transactions on Antennas and Propagation, pp. 709-717, November 1964.

7) J. A. Allnut, *Satellite-to-Ground Radiowave Propagation, Theory, Practice and System Impact at Frequencies Above 1 GHz.* London, United Kingdom: Peter Peregrinus Ltd., 1989.

8) C. M. Rush, E. J. Violette, J. C. Carroll, K. C. Allen, "Impact of SPS Heating on VLF, LF, and MF Telecommunications Ascertained by Experimental Means," NTIA Report Series, U.S. Department of Commerce, April 1980.